August 31, 1998
OSU RF Project Number 732941

Distributed by Ohio Sea Grant College Program as **OHSU-TS-050**. Results of Ohio Sea Grant Project number **R/OE-013**

"Control Algorithm for Underwater 'Wet' Flux-Cored Arc Welding Process"

Final Report

Submitted to

Ohio Sea Grant College Program
The Ohio State University
1314 Kinnear Road
Columbus , Ohio 43212-1194

Submitted by

Dr. Chon L. Tsai, Dr. B.J. Liao, Joseph S. Breeding, David A. Clukey
Department of Industrial, Welding and Systems Engineering
The Ohio State University

Executive Summary

Previous research by Professor Chon Tsai and his underwater welding group at The Ohio State University initiated the adaptation of the flux-cored welding process to underwater "wet" welding. The testing was performed using a shroud consisting of a sponge (to seal the cup to the weldment) fixed on a round cup to create a stable bubble. This enabled the arc to burn smoothly while protecting the weld area from the environment. The results showed significantly improved arc stability and weld appearance. An analysis of microstructures and mechanical properties showed that satisfactory underwater welds could be made using Stoody 308L SOS flux-core wire on A36 mild steel using the local dry spot method.

This project was initiated to further increase weld quality by developing an algorithm to monitor and control the gas cavity dimensions within the shroud to better protect the arc and weld. A microprocessor received thermal data from a sensor in the shroud and converted it into a bubble status message. A semi-empirical relationship between the bubble status message, the test parameters, and weld quality was developed. The test matrix parameters included wire feed speed, welding current, arc voltage, travel speed, and external gas flow. A closed loop control hardware/logic system was developed which used the programmed database. The feed rate was controlled in real time to adjust energy input and hence the amount of gas from the flux and vaporization.

Because of the significant effect of cooling rate on weld properties/microstructures, shroud design was evaluated and a new shroud was developed to slow the cooling rate. It was ovoid in shape, as are the isotherms surrounding the weld pool. The ovoid shape allows the gas shield to flow backwards along the weld centerline to more efficiently shield the weld pool and solidified metal. With the ovoid cup and closed loop system, good bead profiles and sound microstructures were consistently produced. The cooling rate ($T_{8/5}$) was slowed to 4 - 6 seconds from 1.7 seconds, resulting in highly improved hardness and microstructures. No microcracking

was observed in either the weld metal or the heat affected zones. The peak hardnesses were on the weld zone side of the fusion line in the transition region from 308L weld metal to the A36 base metal. Variations in hardness across the weld bead indicate some incomplete mixing of the 304 sheath of the 308L wire and the alloying elements in the flux.

The underwater wet flux-core welding process has been shown to have been successfully integrated with the closed loop arc bubble stabilization software/hardware. The prototype has been successfully refined (based on the test results) so that consistent and quality welds can be made in the small tank. Test coupons for Class A welds have been made in the small tank, but mechanical tests have not been completed. Based on the test results, it is anticipated that the weldments will pass the Class A requirements.

No weldments have been made to date in the dive tank. This was due to moving to the new Welding Engineering building and the subsequent renovations to the tank. The tank has now been refurbished, and test diving in the tank is expected by the end of this year.

ACKNOWLEDGEMENTS

The author would like to acknowledge and thank the many people who contributed either their time, financial resources, or both. Special thanks and recognition go to Dr. Jeffrey M. Reutter, Director of the Ohio Sea Grant College Program and to Dr. Steven G. Olson, Director of the National Coastal Resources Research and Development Institute (NCRI) for their generous and continuing support of the underwater welding projects at The Ohio State University. Their dedication to the research at Ohio State has been instrumental to the success of many projects.

The development of a control algorithm is one of many on-going projects to solve the problems of underwater wet welding, which includes both a fitness-for-service design methodology as well as a materials/process solution using a new electrode dubbed the "Black Beauty". Other projects include a "smart" underwater welding system using feedback loops and through arc seam tracking ability. A virtual vision system is also under development.

Generous support has been received from The Welding Consultants Inc. (William Svekric, President), with financial and material resource contributions. Previous underwater welding in the dive tank and subsequent mechanical tests would not have been possible without Mr. Svekric's generous support. Welding Consultants continues in their dedication to the underwater welding research ongoing at the university.

Special thanks to Ravi Menon from Stoody company for supplying the 308L fluxcore wire used in our research and for his continuing support of this and related projects.

TABLE OF CONTENTS

TABLE OF CONTENTS (cont)

LIST OF TABLES

LIST OF FIGURES

SECTION 1

INTRODUCTION

1.1 Background

1.1.1 Underwater Welding

It has been well established that underwater "wet" welds are subject to rapid cooling and hydrogen embrittlement. Chon L. Tsai and Koichi Masubuchi addressed the mechanics of rapid cooling and their effects in 1979[1] and 1980[2]. Because of their severe impact on weld quality, a brief review is appropriate. For a given material, the composition, peak temperature and cooling rate determine the final microstructure of the heat affected zone. Although the weld metal composition can be controlled to yield a favorable microstructure, the composition of the heat affected zone of the base metal cannot be controlled. Only the cooling rate and peak temperature can be controlled. Figure 1 illustrates a continuous cooling transformation diagram (CCT) with cooling rates typical of underwater and air welding superimposed. As can be seen in typical "wet" welding, the quench effect of the environment results in a martensitic heat affected zone. The hardness is very high and the notch toughness is poor. The microstructure is also subject to hydrogen cracking when atomic hydrogen is present. In "wet" welding disassociated water provides a ready source of hydrogen so control of cooling rate is especially important. As shown in Figure 1, slowing the cooling rate, $T_{8/5}$ to 4.5 seconds yields essentially the same microstructure as for air welding. Different composition base metals change the curves somewhat, and typically a bainite knee is present as illustrated by Atkins[3].

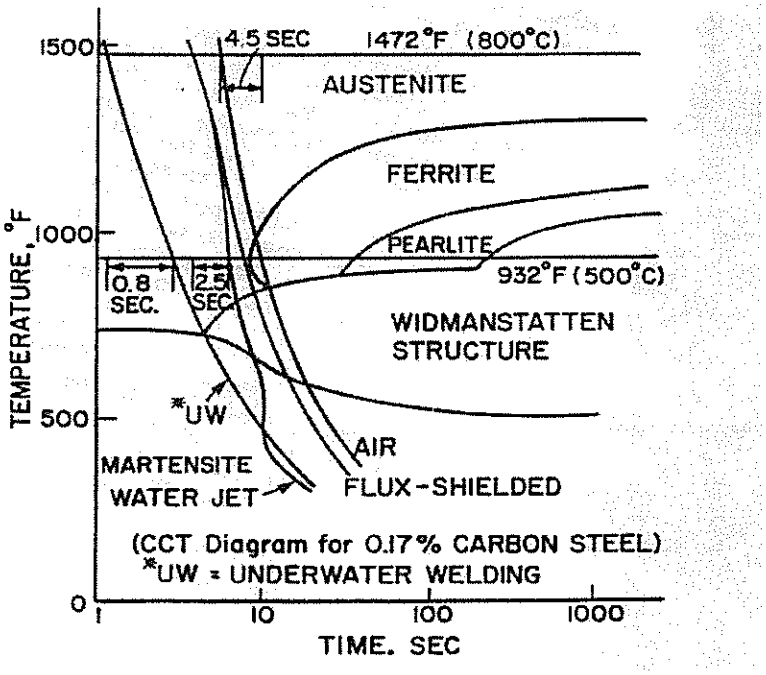

Figure 1-1. CCT Diagram with superimposed cooling rates. Reprinted with permission.

Figure 1-2 illustrates another example of a CCT for steel. The E-Q hardenability curves illustrated by Reference 4 show a drastic reduction in hardness with decreasing martensite content.

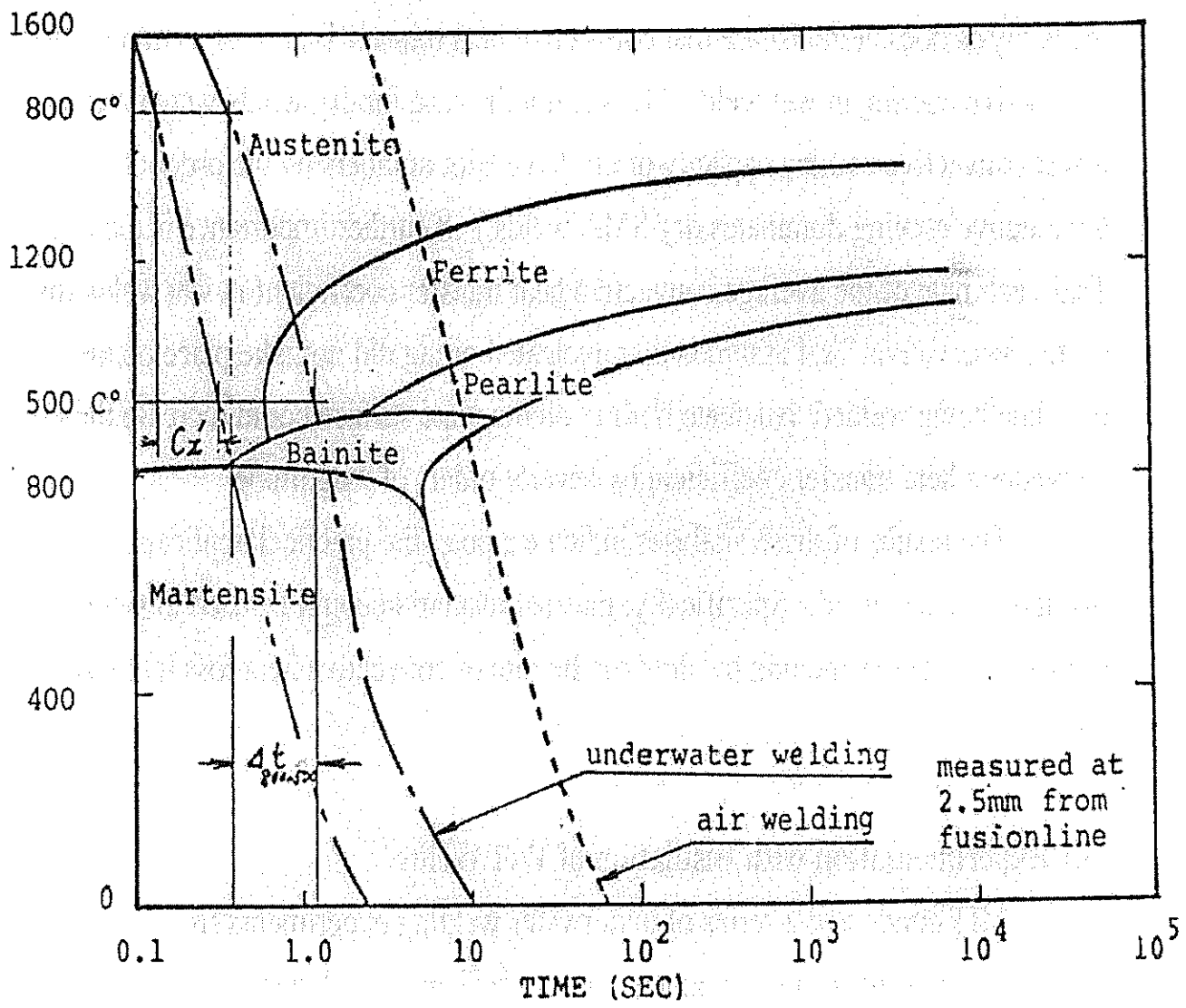

Figure 1-2. CCT diagram showing a bainite region with superimposed cooling curves. Reprinted with permission.

References 5-7 discuss improvements in underwater welding technology. A new underwater welding SMAW electrode was developed and is currently being tested to obtain Class B welds (Ref. 8). With improved fatigue resistance, ease of use, improved mechanical properties, and a fitness for service design approach, many underwater welds can be performed without expensive dry docking of ships or using expensive hyperbaric chambers.

However, there are still many instances were a Class A weld is required. Therefore, someway must be found to adequately slow the cooling rates and reduce the amount of available hydrogen to the weld pool.

1.1.2 Underwater Arc Bubble

According to Tsai[1], the rapid quenching is due to the surface heat loss by convection. In air welding, the heat loss to the air is negligible. However, in water with its higher heat capacity it becomes significant. This is especially so in wet welding because of the dynamic nature of the bubbles which cause the water to flow over the surface of the plate. Figure 1-3 illustrates an idealized bubble. The initial radius, Ro, is the stable part of the bubble and is the smallest radius. As the bubble grows, its radius increases until the height = Ro + Rmax whereupon the dynamic part of the bubble detaches and the void collapses to Ro. This repeated action agitates the water and causes it to flow over the plate. High speed cinematography showed that heat losses were mainly due to heat conduction into the water as is flows by, and that the flow field determined the amount of heat loss. Boiling was observed only in the arc bubble area and not on the plate surface (e.g. no nucleate boiling observed). Masubuchi[2] noted that the heat loss in the dynamic part of the bubble is not fully understood and was difficult to model. It was therefore assumed to be zero inside the heat input circle.

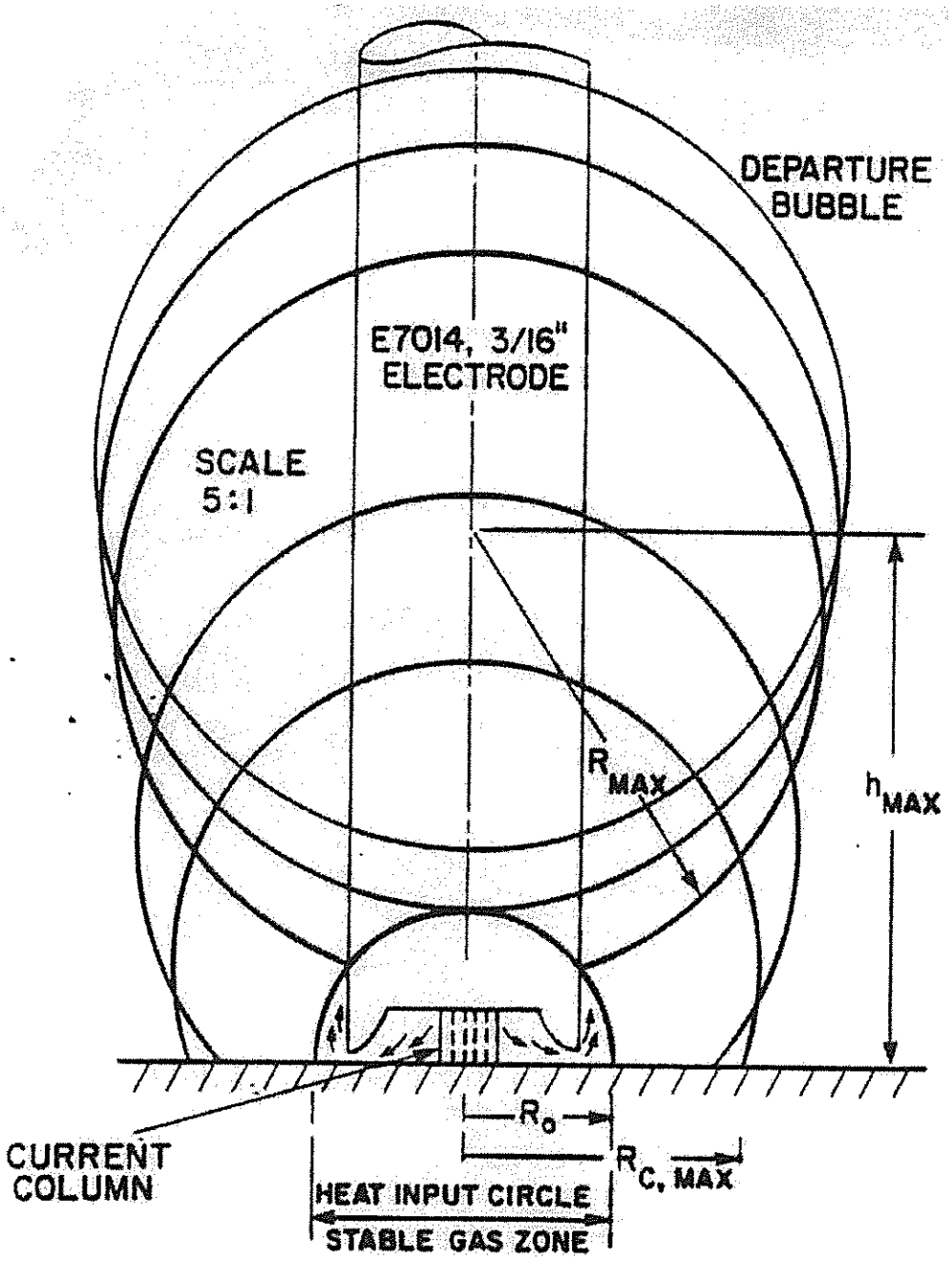

Figure 1-3. Idealized bubble dynamics. Ro is the stable part of the bubble.

Reprinted with permission.

1.1.3 Welding Arc Protection

Because of the detrimental effects of rapid cooling on weld properties, attempts have been made to slow the cooling rates. In early attempts, Tsai[2] looked at arc power, welding speed, base metal thickness, and water temperature. Increasing the arc power from 4000 to 6500 J/S slowed the cooling rate ($T_{8/5}$) by only 0.05 seconds. Slowing the travel speed from 9 ipm to 6 ipm had a more significant effect and reduced the rate by 0.5 seconds (10 times the effect). Increasing the power on thin plates had little effect, but on thick plates increasing arc power slowed the cooling rate by nearly a second. Figure 1-4 illustrates the effect of arc power and plate thickness on the cooling time. The water temperature was found to have little effect on the cooling rate. It was therefore proposed to increase the heat input and slow the travel speed on thicker weldments.

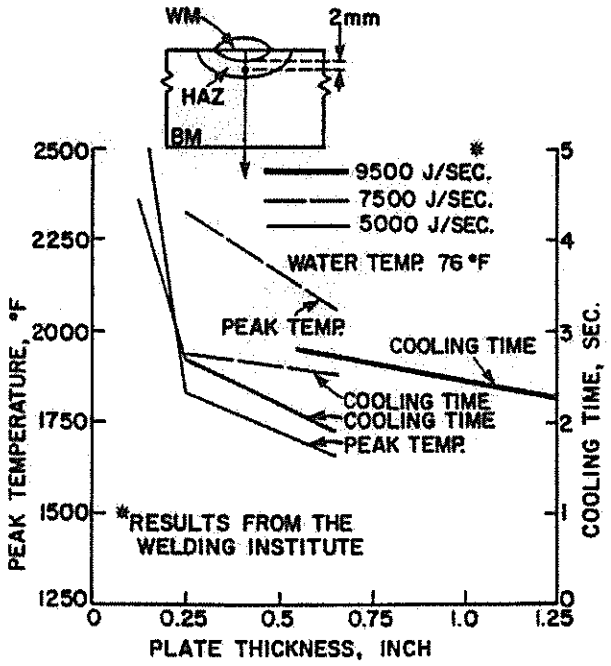

Figure 1-4. Effect of plate thickness and heat input on cooling time (800-500C)2mm from fusion line. Reprinted with permission.

Figure 1-5 shows various attempts to insulate different areas of the plate to reduce the cooling rate. Note that the profiles show that insulating the weld centerline alone had the most dramatic effect on the weld cooling rates.

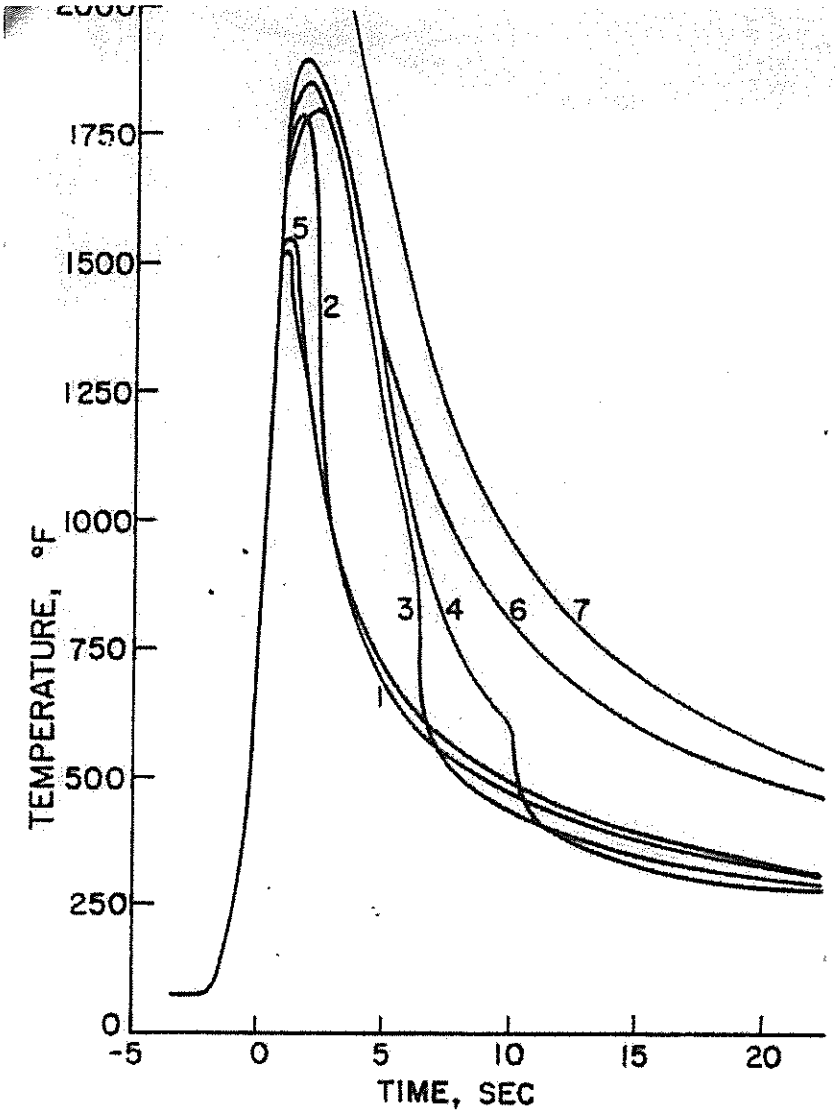

Figure 1-5. Effect of insulation on temperature profiles. 1) R=7mm, 2) R=10mm, 3) R=25mm, 4) R=40mm, 5) all insulated except weld area, 6) weld only insulated, 7) air weld. Reprinted with permission.

Because the weld cooling rates of air welding were not attainable with the marginal decreases in $T_{8/5}$ afforded by the previous mitigation methods, and based on calculations like those in Figure 1.5, efforts were made to protect the welding arc and heat input circle by local dry cavity methods. TIG, MIG, GMAW, and FCAW processes were developed by various organizations with various methods of removing water from the joint. Tsai[1] calculated that there was a minimum Ro to be obtained before deriving any benefit from local dry spot welding. Smaller than that the cooling rate actually increased. This is illustrated in Figure 1-6.

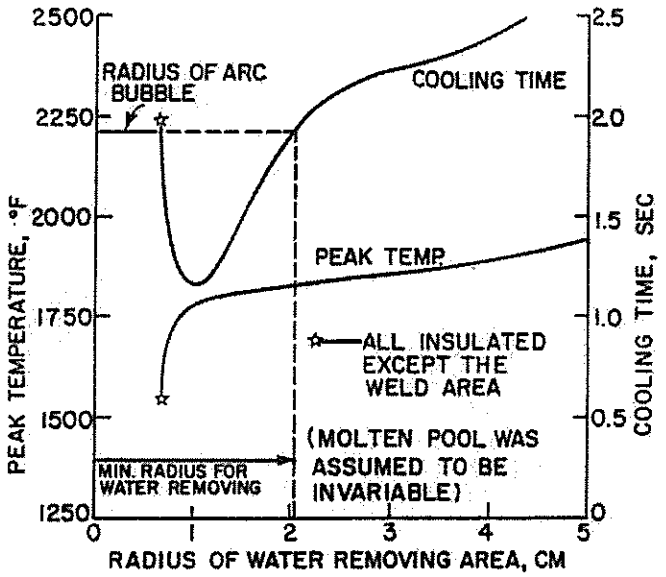

Figure 1-6. Weld cooling time and peak temperature vs bubble cavity size. Reprinted with permission.

The Ohio State University has recently begun a series of projects to develop a flux-core underwater welding system which can produce Class A wet welds. Tsai et.al.[9] in a previous project at The Ohio State University initiated the adaptation of the flux-cored welding process to underwater "wet" welding. A standard flux-core welding gun was waterproofed for the project. Travel speed was controlled by a carriage/side beam system. The system was mechanized to eliminate human factors.

Ferritic (Russian) and 308L austenetic filler metals were tested underwater and compared to air welds. The underwater testing was performed using a shroud consisting of a sponge (to seal the cup to the weldment) fixed on a round cup to create a stable bubble. A trailing "blanket" was dragged behind the shroud to slow the cooling rate of the solidified weld metal. This enabled the arc to burn smoothly while protecting the weld area from the environment. The results showed significantly improved arc stability and weld appearance. An analysis of microstructures and mechanical properties showed that satisfactory underwater welds could be made using Stoody 308L SOS flux-core wire on A36 mild steel using the local dry spot method. The ferritic Russian wire also showed good properties, with the exception of ductility. This was probably due to hydrogen embrittlement caused by high solubility for hydrogen in liquid metal and low solubility upon solidification. Austenetics have a much higher solubility for hydrogen in the solidified weld metal, as well as more slip planes. This gives the austenetics more ductility. However, corrosion may become an issue if a non-matching filler metal is used due to differences in cathodic potentials. Because of the better ductility, 308L was selected for future research.

1.2 Objectives

The objective of this project was to develop a control algorithm to improve weld quality and operating characteristics for underwater "wet" welding. The control algorithm was to be programmed into a microcomputer and integrated with an inverter power supply. The control algorithm was to be developed in the first year. The software program was to be developed and integrated into the welding system in the second year. A prototype system was to be developed and refined by the end of the second year.

1.3 Impacts/Benefits

Successful development of a wet welding process capable of Class A underwater welds will significantly reduce costs when compared to hyperbaric welding (where an artificial air environment is created to produce above-water weld quality). Hyperbaric welding can cost $8,000/hr or more, depending on water depth. Once perfected, the flux-core dry spot welding technique can be used to make permanent repairs to ships, nuclear components, dams, canal gates, and offshore platforms and pipelines. Costly dry docking of ships or expensive hyperbaric welding of offshore structures could be significantly reduced or even eliminated.

1.4 Methodology

In the first year, the hardware and software to monitor the gas cavity conditions for use in a closed loop feedback control system was to be developed. This was performed by a parametric study using wire feed speed, current, voltage, travel speed and external gas flow as variables. Welding tests were performed in 15cm of water in the small tank and compared to air welds. The travel was mechanized eliminate human factors. An inverter power supply and wire feeder were used. Bead on plate tests were performed and cooling rates investigated. Groove welds and mechanical properties were also investigated. The current and voltage hysterisis loops were recorded to indicate the arc stability.

Once the tests were performed, the data were analyzed by visually, mechanically, and metallurgically. The effect of the weld parameters on the bubble stability and weld quality were investigated. Bead appearance, weld porosity, cracking, dilution, hardness, microstructures and mechanical properties were all assessed for conformance to AWS D3.6-93 specifications. The weld properties (e.g. hardness) and microstructures were correlated with CCT curves, and semi-empirical relations were developed for use in the algorithm development.

In the second year, an algorithm was developed to monitor and control the gas cavity dimensions within a shroud to better protect the arc and weld. A microprocessor received thermal data from a sensor in the shroud and converted it into a bubble status message. A semi-empirical relationship between the bubble status message, the test parameters, and weld quality was developed. The test matrix parameters included wire feed speed, welding current, arc voltage, travel speed, and external gas flow. A closed loop control hardware/logic system was developed which used the programmed database. The feed rate was controlled in real time to adjust energy input and hence the amount of gas from the flux and vaporization.

Because of the significant effect of cooling rate on weld properties/microstructures, shroud design was evaluated and optimized.

SECTION 2

EXPERIMENTAL

AND

SYSTEM DEVELOPMENT

2.1 Underwater FCAW System Setup

The underwater FCAW system included the following components: welding power source, wire feeder, welding torch, and welding head carrier for mechanized welding and gas supply for external shielding needed welding. For welding in the small experimental tank (foot-fresh-water, FFW), mechanized welding was used for ease of operation and to eliminate the manipulation errors which occur in manual welding. For welding in the dive tank, diving equipment such as suit, communication gear, and other safety devices are required. If the working depth is less than 10 feet, the wire feeder can be placed on the surface. In the lab, the depth of the dive tank is only 8 feet so the mechanism can be on the surface. When welding in deeper water offshore, an underwater wire feeder is needed.

From the test results of previous research and early tests in current project at OSU, Stoody self-shielding stainless welding wire SOS 308L was used for the filler material in this study. Commonly used low carbon steel (mostly A36) was used for the base metal. Welding research was planed in three stages: in the small tank, in the diving tank, and at remote sites. In this project, the first two stages were included.

2.1.1 Welding System for Test in Small Tank

The small tank dimensions were 30" deep, 48" long, and 36" wide. There was also a transparent view window on the front face of the tank.

The mechanized system used for welding in the small tank consisted of a welding power supply, an automatic wire feeder, a FCAW torch, a side beam, a travel speed control unit, a fume exhaust system, and the fresh water tank. The system is shown in Figure 2-1. Welding could be performed underwater up to 20" deep and travel for 24" .

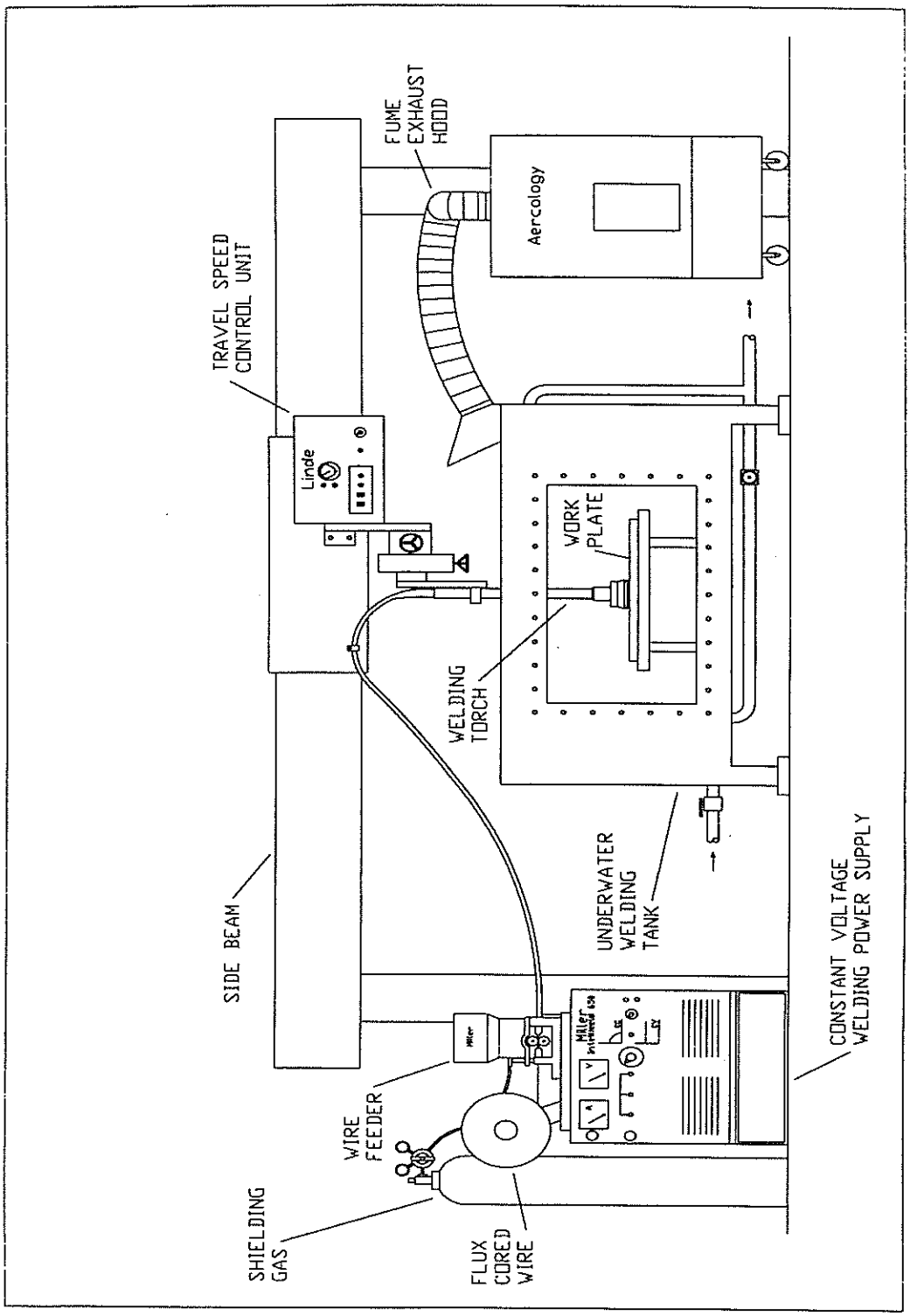

Figure 2-1. Small Tank Underwater FCAW System

The welding power supply was a Miller Intelliweld 650 which could be switched to constant voltage (CV) or constant current (CC). It also supported local or remote start/stop controls and voltage/current settings.

The wire feeder was a Millermatic S-25D model with local or remote feed control. The welding gun used for this project was a modified Miller GA-50A GMAW automatic gun installed on the side beam and connected to the wire feeder with a FCAW semi-automatic cable. A flexible sponge skirt was attached to the nozzle to make a local shroud.

The side beam had speed and direction control as well as vertical and transverse torch position adjustment. The side beam control was synchronized with the welding power supply by a control circuit. This allowed the operator to initiate travel trigger the welding power supply in one motion. The side beam could also move independently if desired.

2.1.2 Local Shroud for Underwater FCAW

One of the problems encountered in underwater wet welding is the shielding of arc and weld pool from the water. One way to overcome the problem was via the local dry spot method. This meant making a local gas environment with the help of a shroud. The function of the shroud was to make a more stable boundary between the gas bubble and the water. With GTAW, GMAW and FCAW, several methods have been developed to shield the arc vicinity such as gas jets, water jets, and wire brushes to make local shrouds. The shroud helps to maintain a gas dominant environment so that the arc burns stable, and metallurgical process can be carried out in a normal manner in the pool. The three gas sources in underwater FCAW are: gas from an external supply, gas from decomposing flux, and water vapor created by the arc heat.

In this study, a flexible sponge skirt with an adapter replaced the standard gas nozzle of the Miller welding torch to make the shroud. With the sponge closely contacting the work surface, a small space was created around the arc and weld pool. Gases passed through this sponge layer slowly and uniformly. External shielding gas helped force water out of the shroud. With self-shielding FCAW, gases from the flux decomposition and vapor filled the whole shroud if the gas-generating rate was high enough and was escaping slowly. A stable gas cavity in the shroud was necessary to make good welds. The advantages of using sponge were: tight and

flexible contact with the work surface, low cost, no special jet mechanisms required, and increased efficiency since there was less external gas needed to maintain the gas cavity in shroud as opposed to the gas jet method.

At first a round (cone) shape double layer bronze cup (for protection from corrosion) was used as the adapter. The sponge layer was clipped between the two bronze layers. In order to reduce the size and ease manipulation, it was remodeled to a single cup with cylindrical shape at the low end. A thin stainless clamp was used to fix the skirt. The designs of the round cup/shroud unit are shown in Figure 2-2 (cup/shroud type C and D). The cup was later remodeled to an ovoid shape (discussed in section 2.4).

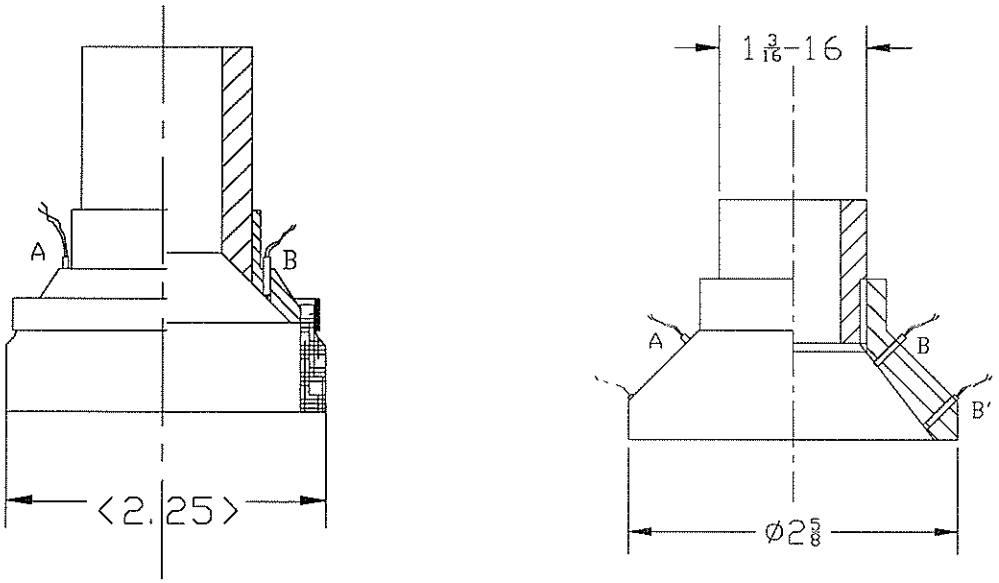

Figure 2-2. Round Gas Cup/Shroud Assembly
Left: Type C; Right Type D

Figure 2-3 shows the shroud holding the gas (external gas flow of 10cfh). A uniform gas cavity filling the shroud can be observed. It was expected that when the sponge was placed on the surface of plate with proper pressure, water in the shroud could be displaced.

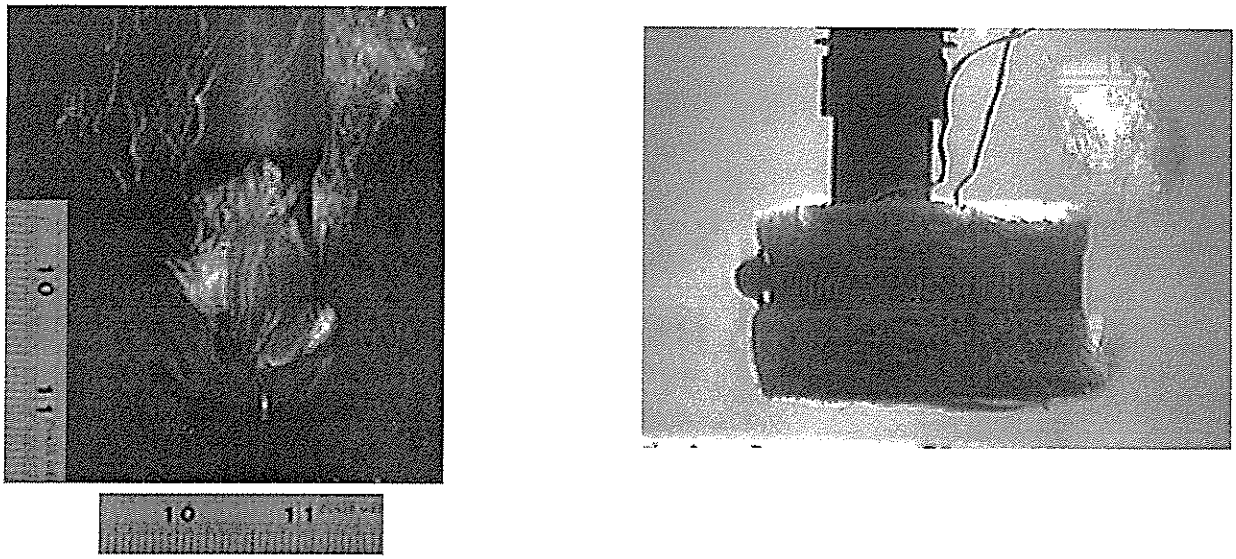

Figure 2-3. Effect of sponge shroud holding gas.
Left: Without shroud, gas flow 60cfh. Right: With shroud, gas flow 10cfh.

2.1.3 System for Diving Welding in Lab

In addition to the basic welding devices, a large tank and accessories will be required. The OSU diving tank is 8ft deep and 8ft in diameter. There are several viewing widows on the wall, and heaters can be used for adjusting the water temperature. A sand filter and pump is used to circulate and clean the water. A knife switch is used to turn on and off the welding power for safety purposes. A picture of the tank is shown Figure 2-4. To conduct semi-automatic welding in the diving tank, two welding guns were connected so it was long enough to reach the work piece in the tank with the wire feeder on the surface. Preliminary tests showed that the wire feeder could feed wire smoothly if the speed was set to the correct speed and the cable/conduit was not curved too much. The tank was moved to the new OSU Welding Engineering Facility this summer from its original location and was refurbished. The diving system is not yet complete, and the planned dive tank welding has not been performed at this time.

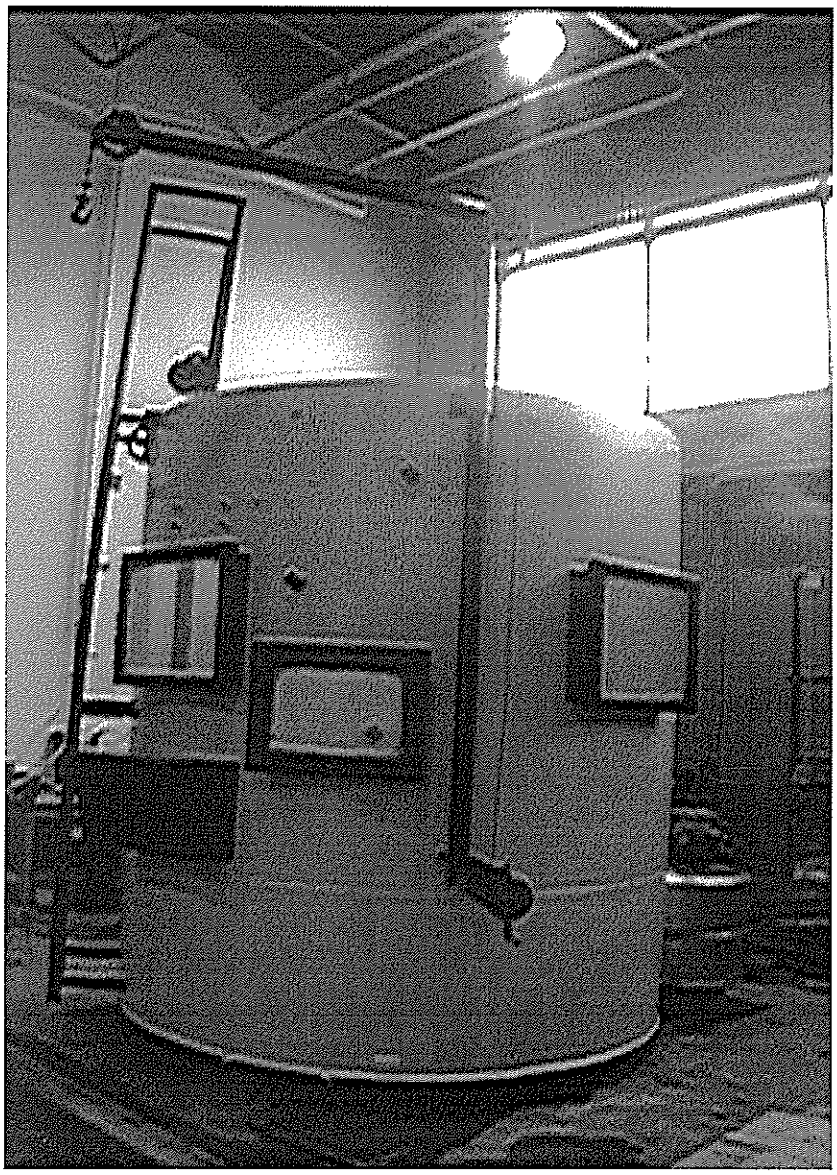

Figure 2-4 Diving tank In OSU Welding Lab. Dia. 8ft; Height 8ft.

A mechanized system will be used in the dive tank. This will improve the welding efficiency since it is difficult to arrange for a diver/welder to perform the welding, and the cost for underwater welding of test coupons is very high. However, it may become possible to bring a diver to the facility at a later time. For lab purposes, most mechanisms will be placed on top of the tank. An operation panel will be next to the view window of the tank. Machining and installation of the motion mechanisms is expected to be finished in three to four months.

2.2 Gas Cavity Status Monitoring

Before developing a control algorithm, a data acquisition system had to be developed. Obtaining dependable and accurate data indicating the state of the gas cavity and its relation to weld quality was an essential element of closed loop control. Therefore, monitoring of the gas cavity surrounding the arc and weld pool by thermal detection was studied. One of aims of this study was to improve weld quality by automatically controlling the gas cavity through adjusting the heat input.

In order to obtain good weld quality, a stable arc is required. With SMAW the arc burns in a bubble consisting of flux generated shielding gas, as well as vaporized and ionized water. Bubble dynamics significantly influences the welding process. With GMAW or FCAW, the arc burns in the shroud. It was found that if the gas volume is enough within the shroud space, the situation is similar to SMAW and dynamic bubbles influence the arc stability. The bubble became to small to protect the pool and solidified weld and cool water from outside the bubble intruded and extinguished the arc. By increasing the gas volume within the shroud, the cavity became bigger and stabled the arc and welding pool. To maintain stable bubble with appropriate size, the gas supply (heat generated or external) had to compensate for the gas lost from the gap between the sponge and work plate and from liquidation of the water vapor.

Many factors affected the gas cavity size, status, and arc stability including: the nozzle (gas cup) or shroud structure, the heat input, the flux amount and type, the external gas flow, the joint type, the water depth, and the welding position.

2.2.1 Gas Cavity Status Sensing Principle

Mass at the welding zone exists in these phases: arc column (ionized gases), welding pool (liquid metal), weld and base metal (solid), arc bubble (gas cavity), surrounding water, and escaping gas. As the arc burns in the local shroud, the arc and gas cavity can not be observed visually. A welder can judge it by leaking arc light and escaping bubbles, but this method is rough and undependable. An electronic vision system may be one solution. However, the main detectable parameters of the media are temperature and pressure, and they can be used to distinguish the gas cavity (gas phase) from the water (liquid phase). This is a more economical solution.

The boiling temperature of water can be reasonably assumed 100°C, when welding in shallow water with about one atmosphere pressure. So the mass must be liquid water where the temperature is lower than 100°C. With several sensors detecting the temperature at different points in the welding zone, the status (gas or water) at these points can be determined and the gas cavity shape calculated. When welding in deep water, the pressure must be considered.

2.2.2 Sensor and Detecting Position

When selecting the thermal sensors, the following factors were considered: temperature range, distribution character, sensor size, accuracy, stability, and durability cost.

An area array device can sense a field temperature distribution and collects much information about the bubble state, but the probe size might be too big for in-torch installation. Also, the welding arc and under water environment is too harsh to this type sensor. It's good for fundamental research, but not for a portable practical welding torch.

As to single point detecting components, semiconductor devices have high sensibility and are good for signal processing and transferring. Heat sensing resistors, diodes, and transistors are examples, but most of these device have lower working temperature ranges, usually around 300°C. In the welding shroud, the temperature may be too high for them when installed near the arc. Furthermore, the welding fumes may affect the accuracy of these types of sensors using radiation principles. Metal heat sensing devices like thermocouples was therefore considered a good choice. Although the sensitivity and signal to noise ratio (with long line connection) are not as high as that of semiconductor devices and reference point setting may be inconvenient, thermocouples have a wide working temperature range and can be used for near arc detecting. They are small enough to install in the gas cup, have good tolerance to environment, and are low cost. In addition, commercial modules for thermocouple signal preprocessing make it easier to transfer signals and set up a detecting system. Although the critical temperature is around 100°C, the temperature in the gas cavity near to the arc may be as high as several hundreds degree Celsius (°C) and hot spatter droplets may attach to the thermocouple tip. Welding thermal detection and air welding test were conducted for comparison, which is much hotter. K type thermocouples with working range 0~1000°C were selected for use in the study.

In order to study the temperature distribution in the gas cup, another testing cup bigger than cup type C was made with more thermocouples installed on it (type D). Four thermocouples were installed near the inner surface of the cup, at front and rear wall at different distances to center and height (see Figure 2-2).

2.2.3 Gas Cavity Monitoring Hardware Design

The data acquisition hardware system is shown in Figure 2-5. It consisted of thermocouples, two thermocouple signal pre-amplifying modules, a welding current sensor, welding current and voltage signal input conditioning modules (which perform amplifying, filtering, and isolation function) and mounting plane, an A/D converter card (installed in computer case), and a host computer.

An IBM compatible personal computer was used as the controller. The DAS-1602 analog I/O interface card featured 16 channels, 12-bit A/D conversion and two channels, and 12-bit D/A conversion. The input ports were set as single end, with reference voltage of 10V (input range is 0~10V), and were digitized to 0~4095.

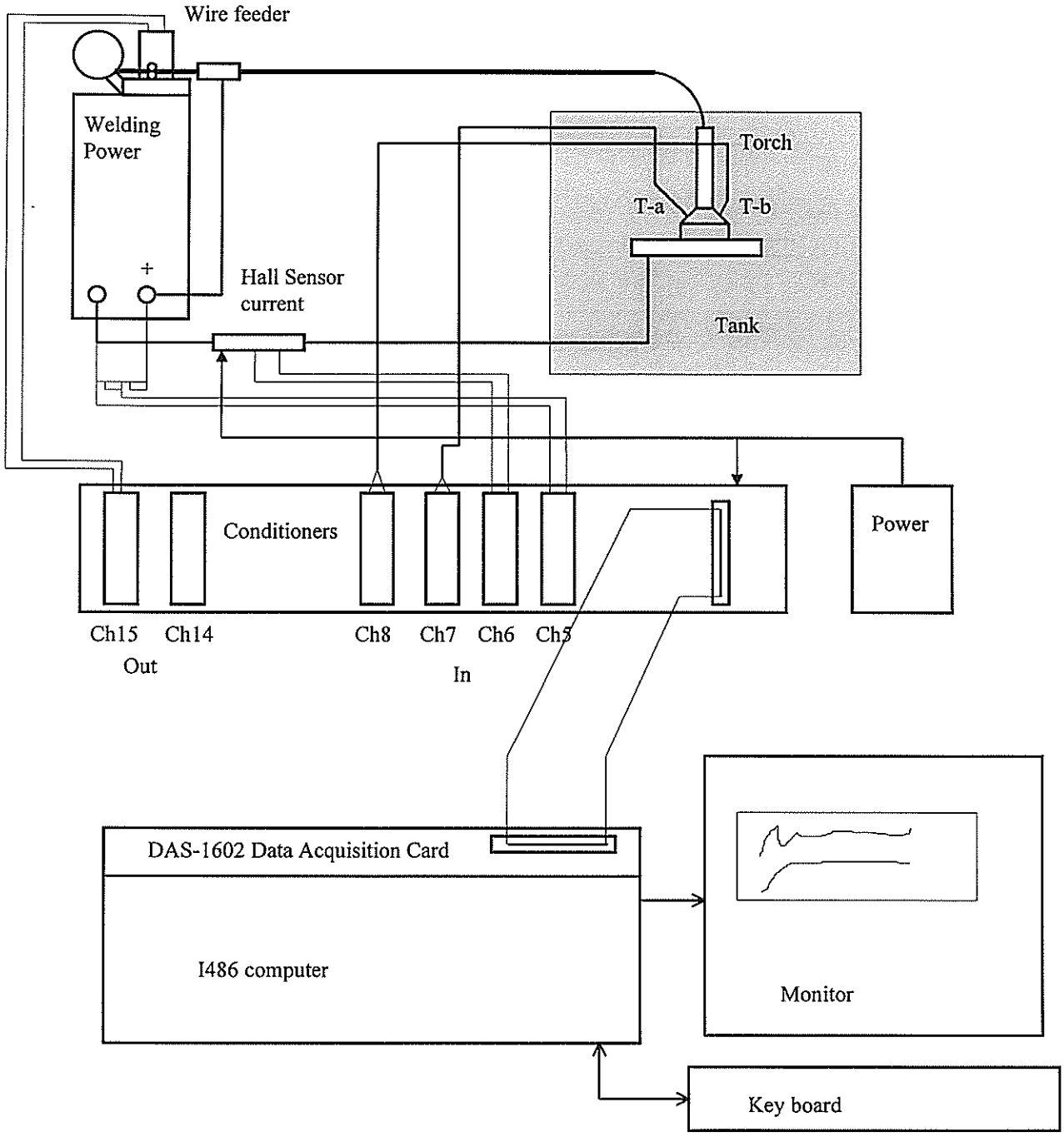

Figure 2-5. Gas Cavity Monitoring/Control System

Arc voltage was detected at power supply terminals. With ladder resistance, a ratio of the voltage (with reduction ratio of 75V to 10V) was input to the conditioning module 5B31 with a ±10V to 5V converting ratio. A CV character power supply was used for FCAW, so a low band module was used.

Arc current was sensed with a Hall effect device, which had no electric connection to the welding power circuit. The transmission ratio was 500A to 50mV, mathematically the same as a shunt for 500A current meter. And then through a ±100mV to 5V signal conditioning module 5B40, the current signal was connected to A/D channel 6. Currents from 0~1000A were converted to digits 1024~2047.

Coated thermocouple wires with welded tips were protected with ceramic tubes to prevent the influence (heat loss) of the bronze cup through which the sensors were installed.

The heat effect voltage at the thermocouple is very low for computer processing. Therefore, the thermocouples (which are conductors) which were exposed to the arc and welding environment were not connected to computer directly because the arc voltage may have damaged the computer circuit. The same applied to the welding current and voltage signals.

Two thermocouple modules of 5B47-K type were installed. The modules converted the weak voltage on the couple to computer compatible 0~5V with a linear correction, that is 0~1000°C temperature input linearly relating to 0~5V output. The sensor at the rear testing point (Point A) in the shroud was connected to channel 7 of the A/D card, and the front point (Point B), to channel 8. 0~1000°C is converted to digit of 0~4095.

2.2.4 Software Development

Gas cavity monitoring software was basically a data acquisition program, but synchronizing power and arc start/stop, data processing, real time graphic display, and saving and retrieving were necessary functions. The program was written with C language. The main procedures of it were:

(1) Sampling of arc voltage, current, and temperature at test points with pre-set programmable frequency. This was possible by using the synchronizing sampling feature of the A/D card and the supporting software. The arc current signal fluctuated seriously because of droplet transfer, so a digital procedure was applied for filtering. The filter formula was:

$$y(n)=(1-\alpha)y(n-1)+\alpha x(n) \quad ;0<\alpha\leq 1$$

with x(n) being the value at the current sampling period, y(n) the filtered result, and y(n-1) the filtered result of last sampling period.

(2) Graphically displaying the arc parameters and temperature detected using a dynamic x-y chart with x indicating time or sampling period and y indicating voltage, current, temperature A and temperature B. When it draws to the right end of the screen, it comes back to beginning of the plot area and overwrites the old plot. The program will not draw the lines when the welding power supply is off.

(3) Data saving. The program could be set to save or not save the data as permanent ASCII format disk file. The file could be used for off line processing and analysis. Only data sampled when the arc is on is saved, except unexpected short time arc extinguishing.

(4) Synchronizing of welding operation, power supply, and arc burning. The logic is as:

(a) If sampled current is less than 20A and voltage less than 8V, power supply is off, otherwise it's on. No arc is defined as arc status 0.

(b) If power is on but the arc isn't = open circuit, defined as arc status 1.

(c) If current is more than 20A, arc is burning. Defined as arc status 2.

The flow chart of the program is shown in Figure 2-6. When starting, the operator was required to set the feeding rate, sampling rate, an data file name.

Another program was written for post data processing and redrawing the waveform. In the data file the average current, voltage, and temperature were calculated. Data sampled at the beginning of arc burning while heat equilibrium had not reached were not counted when calculating the average.

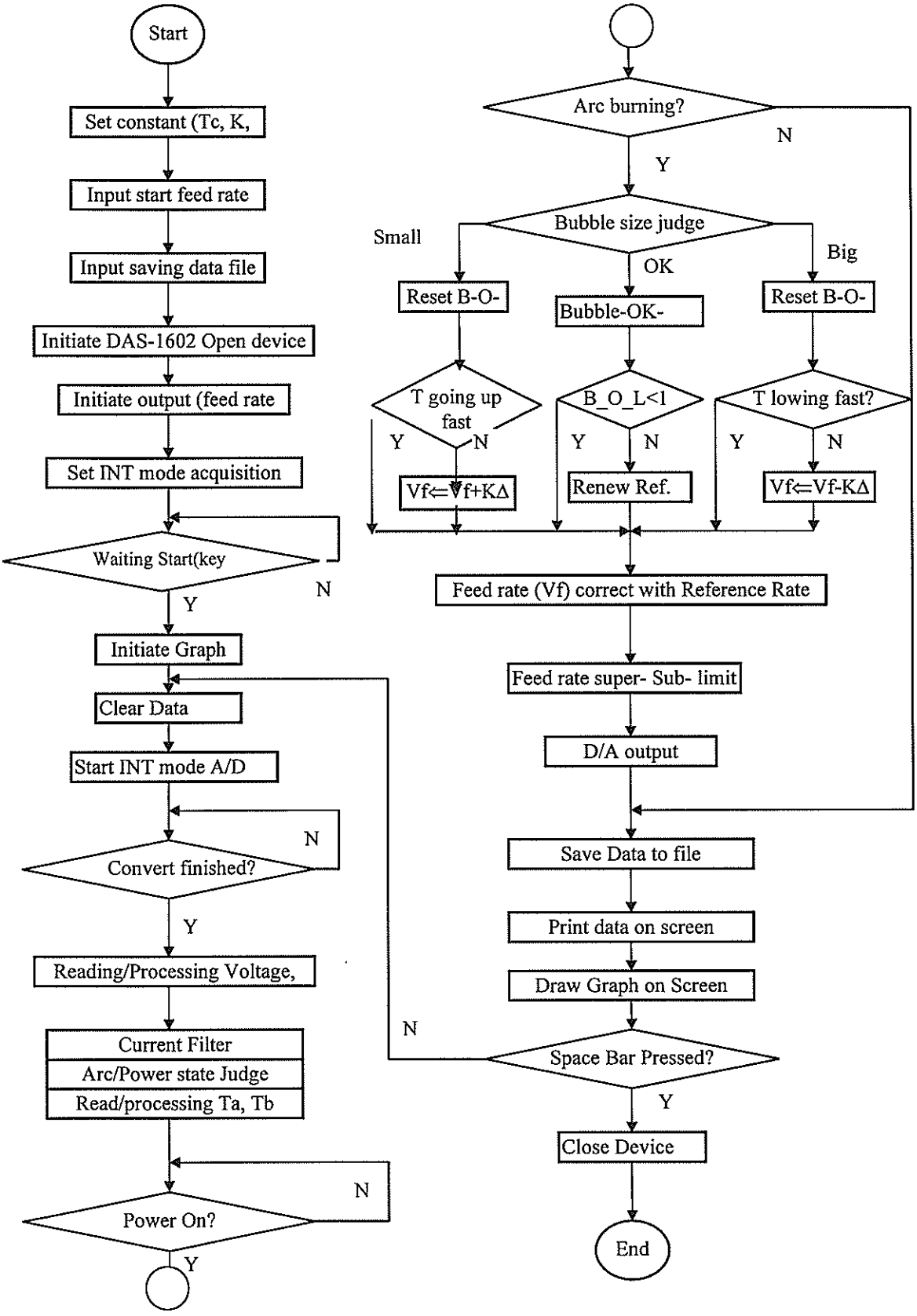

Figure 2-6. Gas Cavity Monitoring/Control Program Flow Chart

2.2.5 Experimental Test Setup

The initial experiments included program adjusting and welding testing. The acquisition system was calibrated by comparing the digitized data and the real values read from the meters. Then the program was adjusted to fit the data range. The sampling frequency was set at 10Hz (with consideration of the dynamic response property of arc bubble and thermocouple) as was the program executing speed.

Figure 2-7 shows the computer screen with the program executing. Data serial numbers, values of feed rates (ipm), current (amps), voltage (volts), and temperature (Celsius) are shown at top line. The five color lines show voltage (yellow), current (white), wire feed rate (cyan) and temperature A (green), temperature B (magenta) waveform respectively.

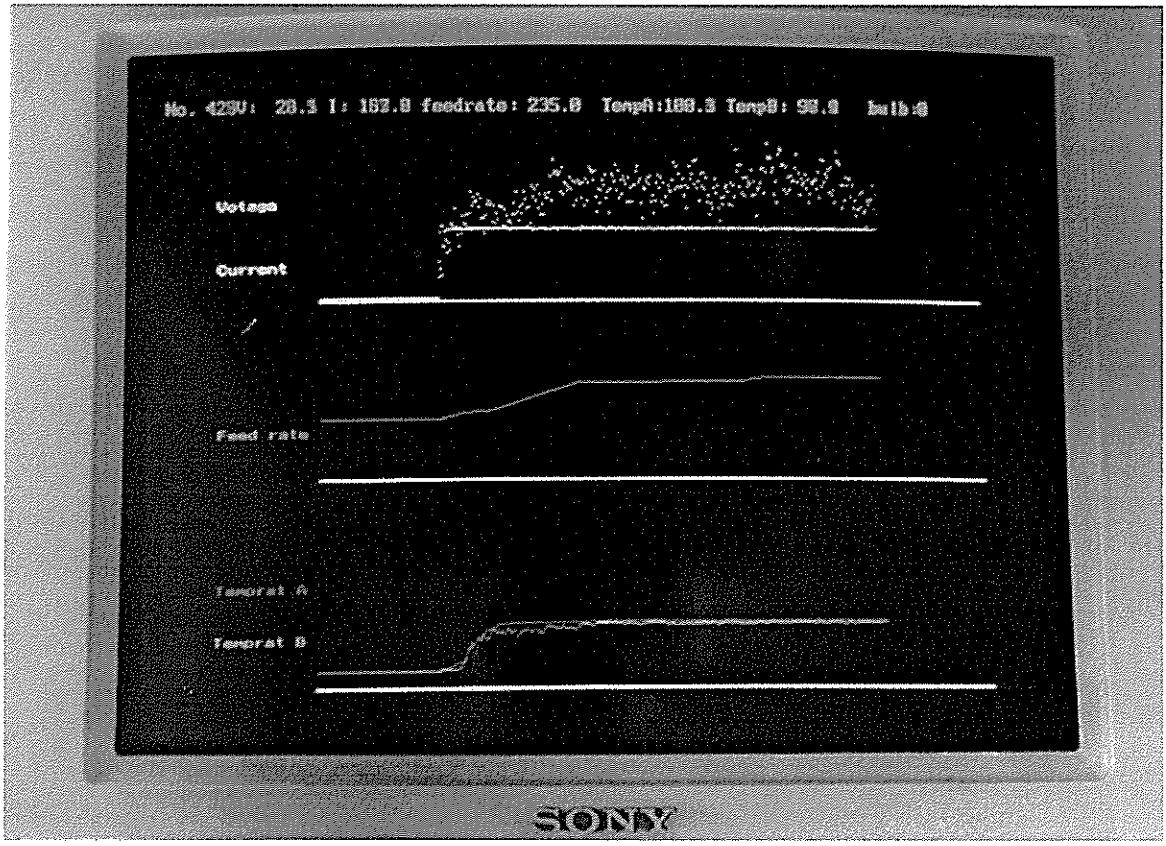

Figure 2-7. Gas cavity monitor/control program executing.
Welding parameter, gas cavity temperature and wire feed rate data shown

Most welding tests were done with about 8" water depth for operational convenience. The base metals were 3/8"~1/2" ASTM A36 steel. According to earlier results, self-shielding stainless flux cored welding wire, type SOS 308L was used with and without externally supplied compressed air.

Welding and environment parameters were:

Arc voltage: 25~32V

Feeding rate: 120~300ipm (ipm)

Welding current: 100~220A

Welding speed: 7ipm~13ipm

Polarity: electrode positive

Electrical stickout: 5/8"~7/8"

Water depth: 8"

Water temperature: 15~32°C

Flat position bead-on-plate welding was conducted in the test.

	No External Gas				Air 7cfh	Air 20cfh	Air 40cfh
	Torch height(in)						
Feed rate	0.625	0.750	0.875	1.000	0.750	0.750	0.750
120ipm		Y					
140		Y			Y	Y	Y
160	Y	Y	Y	Y			
180		Y					
200	Y	Y	Y	Y			
220		Y					

Table 2-1. Gas cavity temperature test matrix

The following test groups were performed for comparison and to obtain data for setup model. Table 2-1 shows the test matrix.

Group 1. The relationship of welding current, weld appearance and cavity temperature. In this group, welding performance, weld formability and detected temperatures of welding with different wire feed rates were compared.

Group 2. The temperature distribution. Temperatures of different test points were compared and used to create a model.

Group 3. Effects of shroud tightness. This test was to be conducted by change the torch to work distance.

Group 4. Effects of external gas flow on cavity temperature and weld quality.

2.3 Control Algorithm Development

After creating the data acquisition hardware and calibrations, an algorithm was developed for real-time control of the gas cavity status. A real time closed loop system to control the cavity size was implemented by adjusting the gas supply (arc heat induced or external gas).

The results of gas cavity monitoring indicated that two thermocouples, with one thermocouple embedded at the rear (point A) and the other at the front (point B) of the cup, could indicate the size of the gas cavity. With appropriate position, the former defines the minimum needed bubble size, the latter defines the largest size needed with close-loop control.

Once the cavity size was detected by the temperatures at the two test points, the energy input was adjusted to produce the required gas volume and cavity size. The study included control logic, control parameter selection, and hardware/software development.

2.3.1 Control Parameter

In the control system, the bubble or gas cavity status was the output of the system, with the temperature at the two testing points the sensed value of cavity status. While the adjusting parameter was arc current, welding speed, gas flow, and other factors affected the bubble status. Considering the three factors deciding energy input, arc voltage can not vary much, and welding speed cannot be changed quickly because of the side beam carriage inertia. Arc current, which is mostly decided by wire feed rate, was therefore the main parameter affecting gas cavity size. Besides, wire feed rate is easier to adjust than welding speed.

2.3.2 Hardware Design

The wire feeder could be switched to remote setting feeding rate. The needed value calculated with control logic was converted to an analog signal at the D/A output port, then connected to a conditioning module, the output of which was connected to the wire feeder.

The D/A converter was built into the DAS-1602 interface card, featuring 12bit. The reference voltage was set at 5V, single polarity (digit 0~4095 converted to 0~5V). The output module had a transmission ratio of 5V to 20mA. A 250Ω resistance was used to convert the current signal to the voltage signal that was required by the wire feeder.

In the study of close loop control, shroud type C was used which was of smaller size. The detecting points (A and B) were nearer to the arc than that of type D shroud, so it could confine the bubble size better.

The system was constructed based on the gas cavity monitoring system, with an additional output interface and wire feeder control unit. The diagram is shown in Figure 2-5.

2.3.3 Control Logic and Software Development

The control logic is : if gas cavity (arc bubble) size is small than required minimum, increase feed rate. If the size is bigger than needed maximum, decrease feed rate.

It is difficult and unnecessary to tell accurate cavity size, but it can be judged by the test temperatures at points A and B. By serial experiments measuring arc stability and weld appearance, and analyzing the relation to the detected temperatures, the following logic has been chosen: if temperature at point A (T_a) is lower than low critical temperature (T_{c1}), the bubble size is too small; if temperature at point B (T_b) is over a critical temperature T_{c2}, and Ta over a high critical point $T_{c3,}$ bubble is over size.

Basically, the control algorithm is: if bubble size is small, feed rate is changed as:

$$V_f(n+1) \Leftarrow V_f(n) + K \bullet \Delta$$

If bubble size is large, feed rate is changed as:

$$V_f(n+1) \Leftarrow V_f(n) - K \bullet \Delta$$

Here $V_f(n+1)$ is the new feed rate, and $V_f(n)$ the old value. K is a constant considering the respond speed of the whole loop.

At first, a PI (proportion-integral) regulation, the most common control rule was applied, that is Δ defined as T_a-T_{c1}. But experiments showed that it didn't work satisfactorily. One of the reasons was that the cavity size and temperature relation was not linear.

Because the PI regulation didn't work, a step control regulation was used. Δ is defined as a constant: 10ipm (inches per minute). Only if the bubble size was out of range would the feed rate change a definite value at an adjusting period, with K as proportional factor. The factor K

and adjusting period Δt have critical effects on the response of the close loop. Δt set to 0.1s was proved reasonable by experimental results. K is to be set when executing the program, and a value of 0.05~0.2 worked well with the usual welding parameters.

An automatic search for optimized feed rate was also introduced into the control program. A value $V^*_f(n)$ with which good bubble status was reached in the recent ten adjusting periods was defined as "good value" V_{fg}. The actual feed rate is adjusted as:

$$V_{f0}(n+1) \Leftarrow V_f(n) \pm K \bullet \Delta$$

$$V_f(n+1) \Leftarrow (1-\beta) \bullet V_{fg} + \beta \bullet V_{f0}(n+1);\ 0<\beta \leq 1$$

With β=0.5, this control logic obtained good control results. With welding torch height, shroud condition, voltage, travel speed determined, the feed rate was optimized to a stable value quickly and the gas cavity was maintained stable with the control program.

At the beginning of welding, the shroud was filled with cold water. It took a few seconds for the arc to warm the water and establish a gas cavity. Even through the heat input was high enough the temperature rose gradually. The above control logic didn't apply to this occasion. Supplemental logic was introduced: while "bubble is small" but temperature rises quickly, the feed rate will not be increased. And, if "bubble is too large", but temperature is going down rapidly, there will be no feed rate decrease.

The program flow chart is shown in Figure 2-6. While beginning the program, the operator was asked to set the starting feed rate, control ratio, and if the data is to be saved to a file. If so, the filename must be input. Appendix A shows the control program.

2.3.4 Close Loop Control Test Setup

The first series of tests were bead-on-plate in the flat position. These experiments were to confirm the function of the control algorithm. The starting feed rates were set random. The feed rate adjusting history and weld appearances were studied. The butt joints with V groove were welded with this control system.

2.4. Post Weld Protection And Cooling Rate Control

The quench effect of water resulted in high weld and HAZ hardnesses, and hydrogen induced cracking was observed. Cooling rates of underwater welds are known to be as fast as 2~3 times that of surface welding. The reason is insufficient heat shield for the just solidified metal.

2.4.1 Gas Flow Control by Shroud Design

The cooling rate of weld and HAZ was affected by heat input, external gas volume, and shielding shroud. Once the shroud passes the weld, the shielding gas escapes and liquidates quickly and cool water will pour down to the weld. If the rear part in the shroud is lengthened and an adequate outlet is provided at the rear end, the hot gases can be guided to the rear part of the shroud and collected around the weld. Ovoid flexible shroud prototype (cup/shroud type E) was therefore made. Cooling time from 800°C to 500°C, $T_{8/5}$, is critical to ferrous steel phase transient (base metal). The shortest distance from the pool rear edge to the shroud rear wall divided by the travel speed is the time for a good $T_{8/5}$. It was therefore adjusted by welding speed and heat input. Considering the shielding effect, manipulation, and machining/installation factors, several designs were made. They are shown in Figure 2-8.

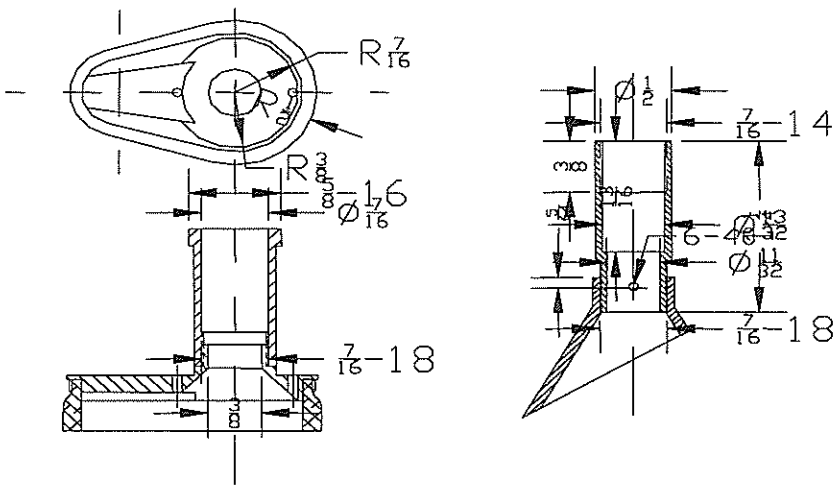

Figure 2-8 Ovoid shroud designs. Left: for mechanized welding; Right: for semi-automatic welding

2.4.2 Cooling Rate Control and Weld Protection Test Setup

Temperature variations in the HAZ near to fusion line were used to compare cooling rates with different shielding methods. The cooling rate at the front surface of the work may be influenced by shielding type most seriously, but it's very difficult to attach thermocouples to the correct position near the weld toe. Because of the steep temperature gradient, temperature measurement was very sensitive to the distance from test point to the fusion line. And since the toe line of weld bead was not uniform, the thermocouples were likely to either be melted off or be too far away from fusion line for pertinent information. To avoid this problem, the thermocouples were attached in blind holes at the back of work plate. With testing, the effect of each welding parameter on penetration was measured. These depths determined the depth of the blind holes used for thermocouple measurements. The holes were accurately made on a drill press. Slight deviations from the center line of weld bead would not influence the distance of the thermocouple tip to fusion line as it might on the top surface of plate, because of the shape of the bead cross section.

Several kinds of shielding nozzles and cup/shrouds and different welding parameters were tested. Included were a standard Miller nozzle in air, underwater, round cup, ovoid cup/shroud in water, and different external gas flows. The test matrix is shown in Table 2-2.

Gas flow (Air, cfh)	0	7	60	70
In Air	Y			
Underwater No Shroud			Y	
Underwater Round Shroud	Y			
Underwater Ovoid Shroud	Y	Y		Y

Table 2-2. Cooling rate test matrix

2.5 Design Of A Commercial Prototype

Based on the results of the control algorithm study with mechanized welding in the small tank, a commercial prototype used for semi-automatic underwater welding was designed. In this design, A standard semi-automatic FCAW welding torch was remodeled. A pair of reed-magnet switches replaced the original ones for waterproofing purposes. The nozzle was changed from a cone cup to an oval opening with a sponge fixed as a shroud. Two thermocouples were embedded in the cup. This cup was designed for welding with a drag angle of 30°, which is the common for FCAW, and it improved the weld contour. Figure 2-9 shows a photo of the torch. The torch can currently be used in OSU diving tank by a qualified diver. It could be further modified and waterproofed for use in an open environment.

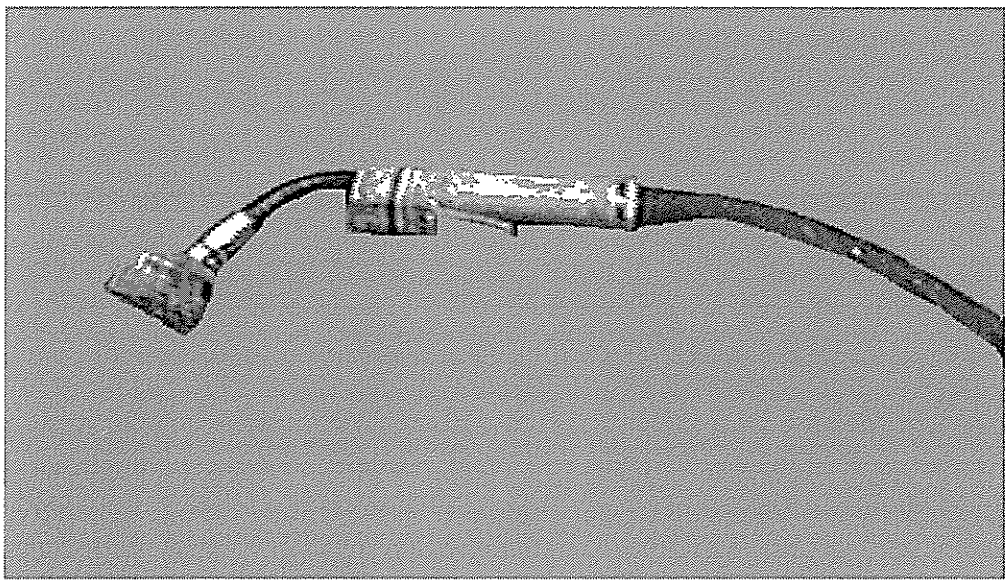

Figure 2-9. Prototype of semi-automatic underwater FCAW torch with two thermocouples embedded in ovoid sponge shroud. Arc bubble monitored and controlled by a Motorola M68HC16Z microcontroller.

In the prototype system a Motorola M68HC16Z microcontroller based circuit board was used instead of the desktop PC. It integrates analog, digital input and output ports. Welding parameters and cavity temperature signals are sampled by an embedded A/D converter and processed. Its output will show the status of gas cavity and control the wire feeder speed. With the size of 4" by 6.5", the board can be packed and sealed in a small box for underwater use. The controller can also communicate with a PC, so the data can be transferred to a PC for post analysis.

An optional visual guidance subsystem was also created for the prototype (this was not a planed task of this project). A small waterproof CCD (charge couple device) camera head can be mounted through the cup wall to take the image of the groove before the arc. With the design of a filter lens, ceramic fiber insulation, and mechanical assembly, the camera head can work well in the underwater arc welding environment. The camera outputs a standard NTSC video signal, which can be transmitted to an eyepiece video screen installed in the diving helmet. At this point, the display still needs to be integrated with the diving helmet. The camera head has a size of only 3/8" diameter and 1.6" long.

SECTION 3

DISCUSSION

of

BUBBLE MONITORING/CONTROL

and

WELD PROTECTION TEST RESULTS

3.1 Welding Parameters for SOS 308L FCAW Wire

These test results established a database for FCAW process using this type of filler metal.

3.1.1 Relation Between Welding Current and Wire Feed Rate

It is well known that with a CV character power source, welding current is decided mainly by feed rate, and the arc length is decided by voltage. With the 1/16" diameter SOS308L self-shielding flux-cored wire used in this study, currents for different feed rates are shown in Table3-1.

The tests were done with the arc voltage about 27V, and tip-to-work distance about 0.75". The relation between average current and feed rate can be described by the equation:

$$I=0.707V_f+21$$

where V_f is in inches per minute, I in amperes. Voltage and tip-to-work distance also affect the current.

Feed Rate (ipm)	120	140	160	180	200	220
Average Current	103	122	138	150	162	178

Table 3-1 Welding currents at various feed rates

3.1.2 Effects Of Welding Parameters on Weld Soundness

Figure 3-1 shows the appearances of the weld beads with different currents. Weld penetration, toe angle, and surface smoothness of the beads were used to evaluate the weld soundness.

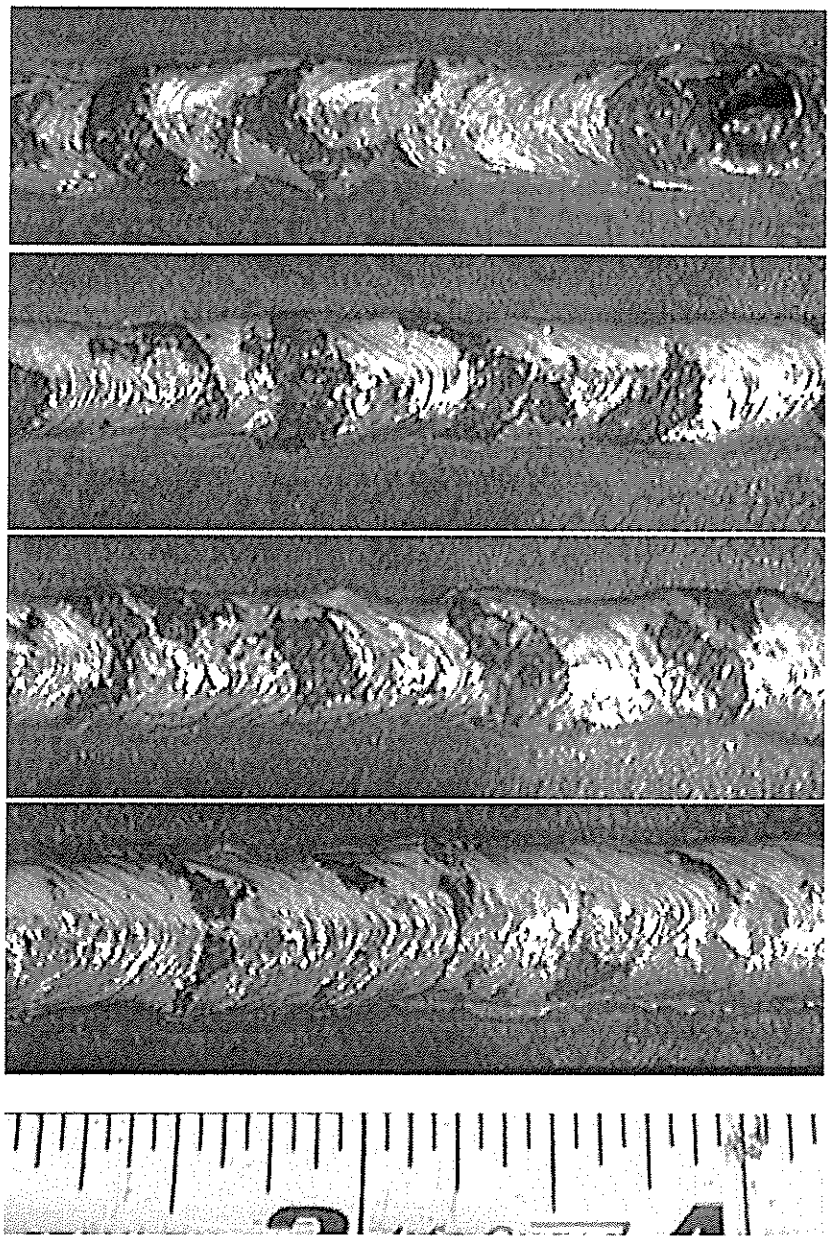

Figure 3-1(a)~(d) Appearance of welds with shroud at different feed rates
a). 1st from top, 140ipm;
b). 2nd from top, 160ipm;
c). 3rd from top, 180ipm;
d). bottom, 200ipm

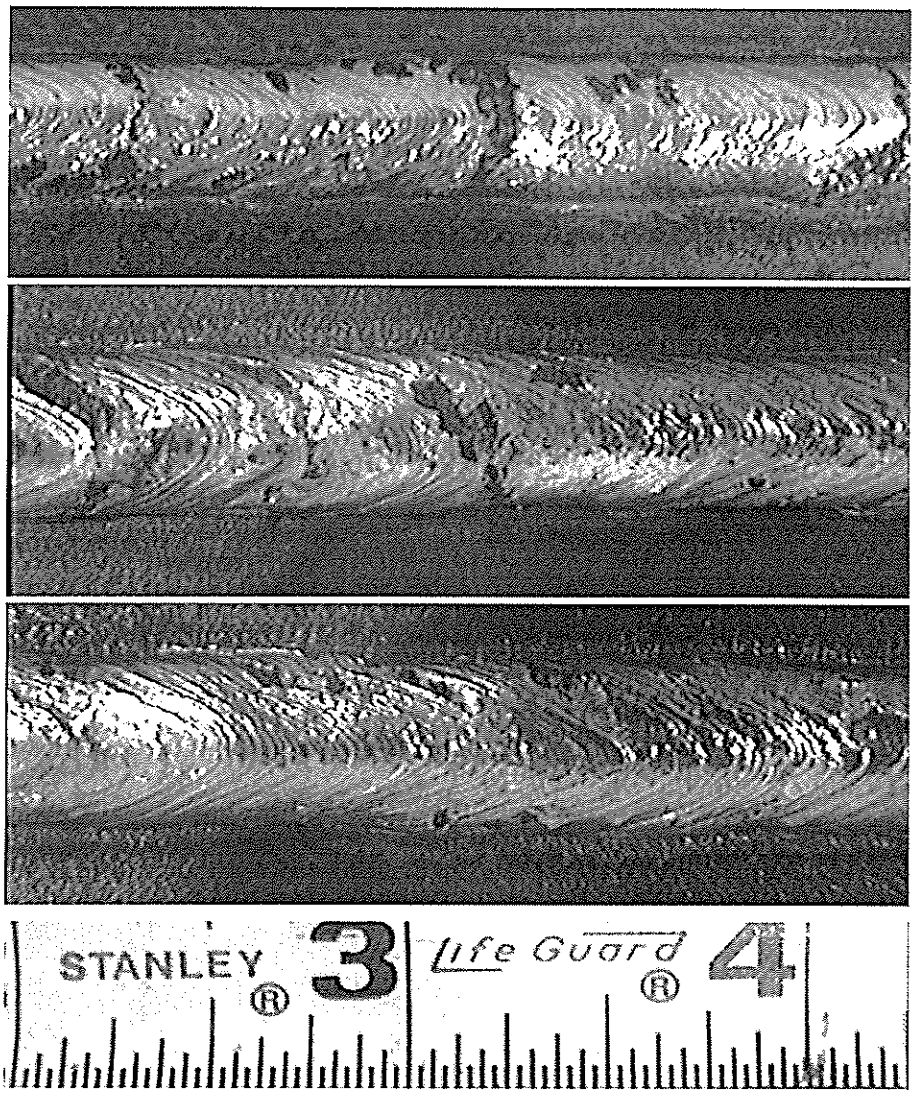

Figure 3-1(e)~(g). Appearance of welds with shroud at different feed rates
e). top, 220ipm;
f). middle, 250ipm;
g). lower, 280ipm;

The black "scars" on the surface were found to be mix of oxidized metal and slag. Under these scars, large pore porosities were likely to be found. Low welding current resulted in inadequate self generated shielding gas to properly shield the weld pool. Also, the energy input didn't vaporize enough water to keep the liquid water far enough away from the arc and pool. Occasionally, water intruded and was vaporized by the pool making the oxygen and hydrogen partial pressures high. This resulted in abnormal solidification and the creation of the scar like spots. Most spots were found in low current welding conditions.

Appearances of welds at feed rates lower than 160ipm (currents lower than 145A) were usually poor. With feed rates of 160~200ipm(current 150 to 175A), acceptable profiles were produced when the sponge shroud was in good condition. At feed rates more than 240ipm (till about 360ipm, currents more than 190A), very good weld appearances were obtained. Porosity, microstructures, and mechanical properties are discussed in Section 4.

3.2 Relation between Arc Bubble Temperature and Welding Condition

Several groups of tests with different wire feed rates, torch height (tip-to-work distance), gas flows, detecting points, and shroud shapes were conducted to establish a relationship between the variables and to optimize parameter settings and shroud design.

3.2.1 Relationship of Gas Cavity Temperature and Current

These welding tests were performed with D type gas shroud, no external shielding gas, welding speed 10ipm, water depth 8", wire stick out 0.75", and the bottom of the sponge skirt slightly contact to work piece. Feed rate varied from 120ipm to 240ipm. Detecting points were A, A', B, B' near the inner face of the bronze cup.

Table 3-2 shows typcial temperatures at different test points and current (feed rate).

Feed rate (ipm)	Current (A)	Ta (°C)	Tb (°C)	Ta'(°C)	Tb' (°C)
120	103	88	64	105	73
160	140	95	75	125	80
200	170	97	77	136	80
240	195	98	86	137	93

Table 3-2. Temperatures at various test points (D shroud)

Figure 3-2 contains the welding parameter and bubble temperature records of all welding for this test group. From the waveform it can be found that the current was low, the detected temperature was low, and the weld contour was poor.

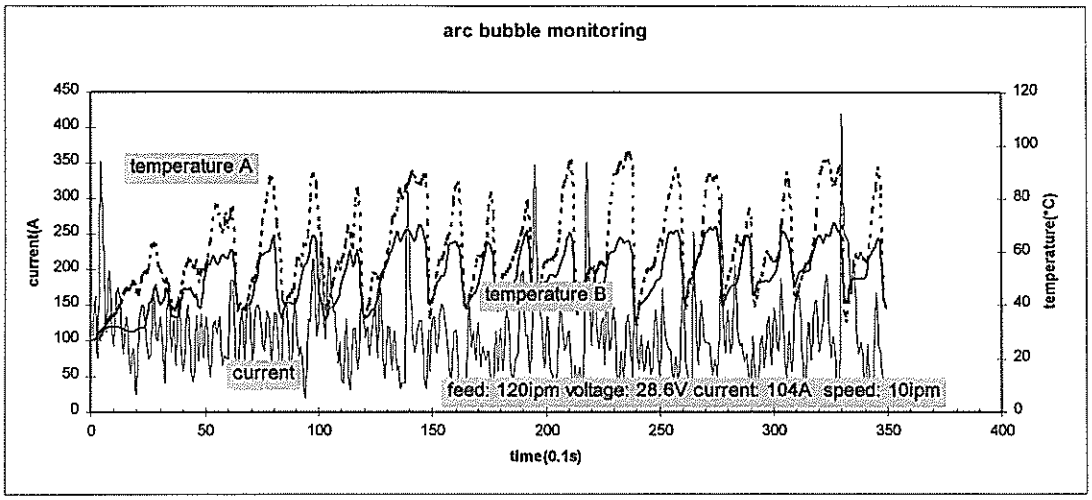

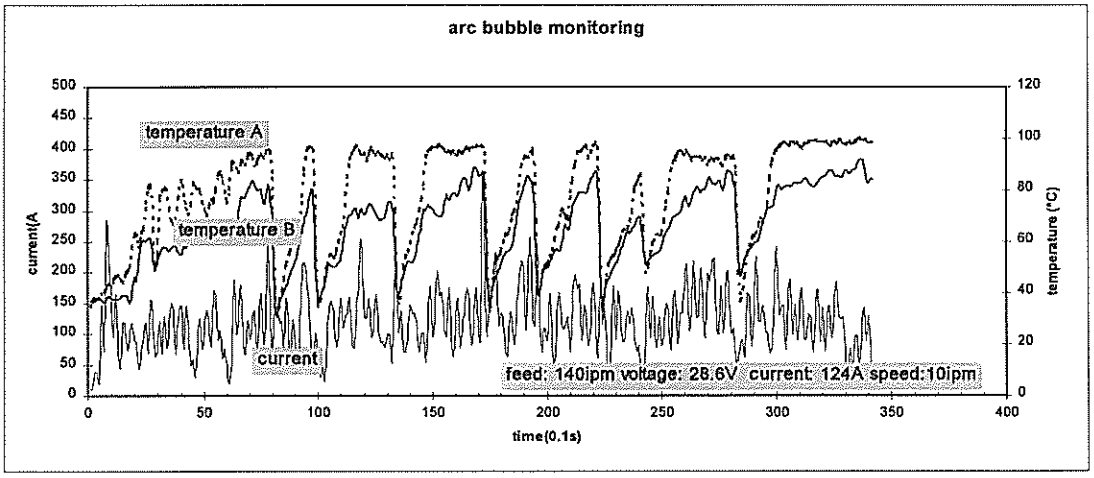

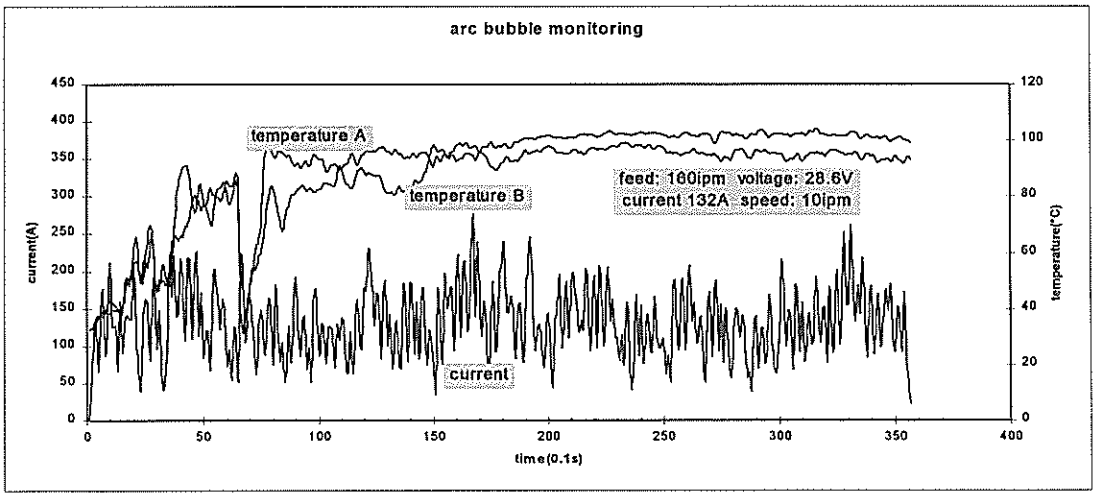

Figure 3-2(a)~(c) Gas Cavity Temperature Vs. Arc Parameter Records

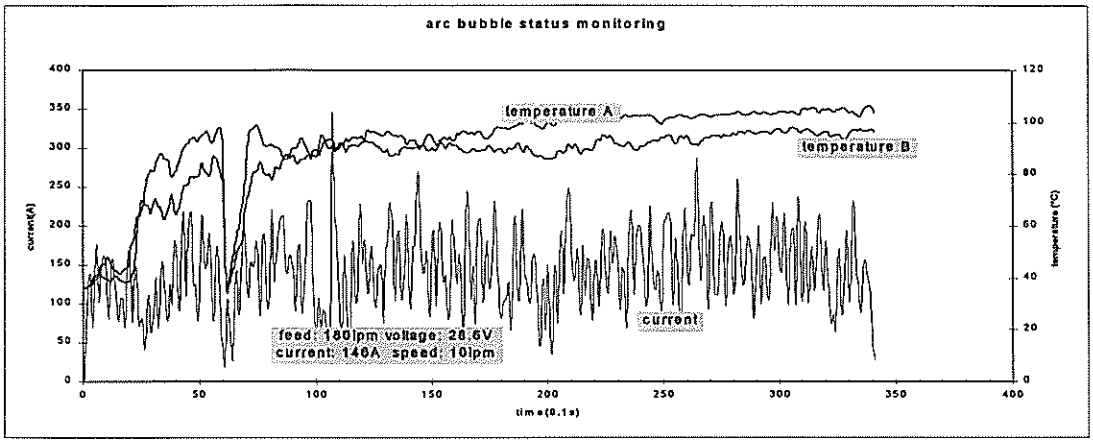

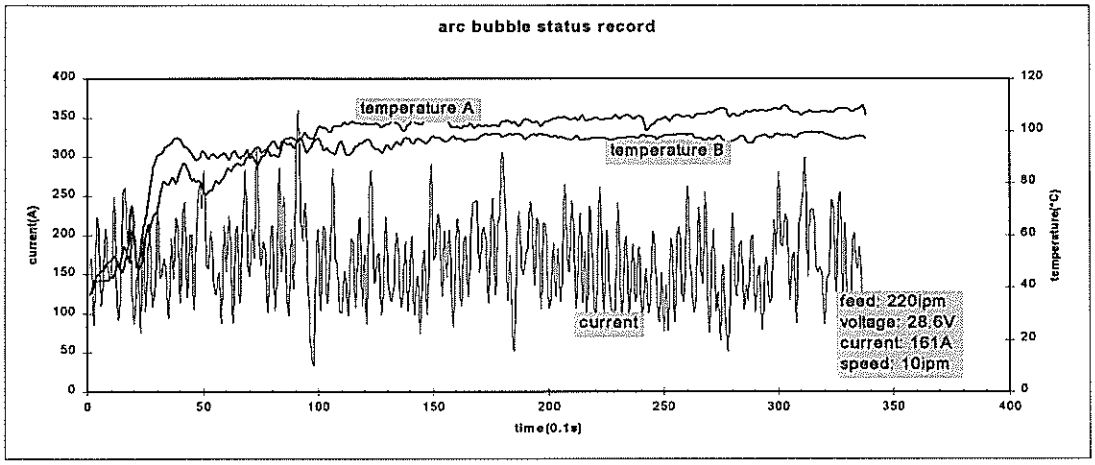

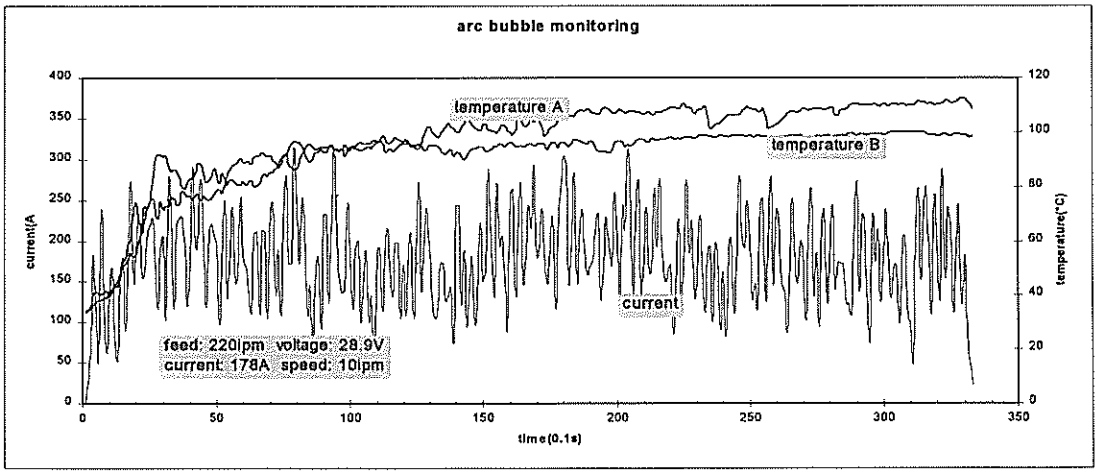

Figure 3-2(d)~(f) Gas Cavity Temperature Vs. Arc Parameter Records

Figures 3-2(a) and (b) show the results of welding with very low feed rates of 120ipm and 140ipm (currents less than 120A). The serious temperature fluctuation was caused by insufficient gas supply. The detecting points were at the unstable boundary of gas and liquid phases. The weld appearances were not satisfactory.

With feed rates more than 160ipm or currents more than 130A in this group, arc energy was nearly enough to establish and maintain a larger stable gas phase around the arc and pool. The boundary was outside the detecting point, so detected temperatures were more stable and rose to nearly 100°C. Smooth weld contours were obtained using these parameters.

Different groups of tests showed similar results. However, when feed rates were low different temperatures were detected with the same feed rate in different groups. With higher feed rate, results showed good repeatability. The reason was that for different groups the sponge skirt covered the work plate with different tightness and resulted in different gas holding effect. Although the temperatures detected might have varied with the same feed rate, the test proved that the average temperature shows high correlation to weld appearance and contour. The higher the temperatures detected in welding, the better the weld appearances. Figure 3-3 shows the relation between current and temperature.

file name	Voltage	FeedRate	current	orchHeig	Deepth	GasFlow	Ta	Tb	Ta'	Tb'
(*.dat)	(V)	(ipm)	(A)	(in.)	(in.)		(*C)	(*C)	(*C)	(*C)
521E		120	102				87.6	64.4		
521F		140	121				90.9	69.6		
521G		160	139				94.5	74.6		
521H		180	155				97.8	75		
521I		200	162				96	77.1		
521J		220	171				98.3	87.7		
521K'		240	187				98.2	85.5		
521L		120	103						105	72.7
521M'		160	144						125.1	79.3
521N		200	176						135.6	80.1
617A		120	104				53.1		63.1	
617B		140	124				68.9		79.9	
617C		160	132				92.9		99.2	
617D		180	146				91.9		99.3	
617E		200	161				96.5		104.1	
617F		220	178				96.5		104.8	

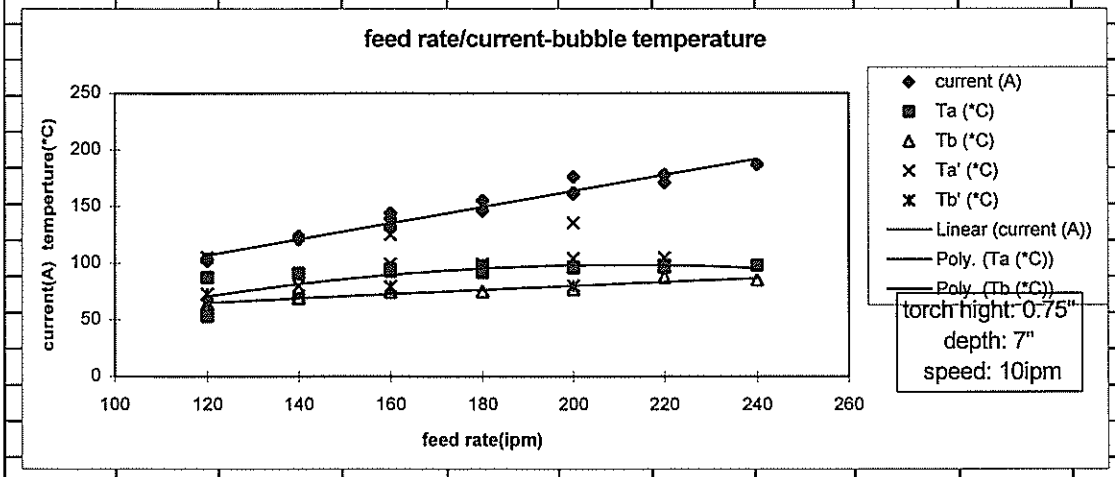

Figure 3-3. Gas Cavity Temperature-Feed Rate Correlation

3.2.2 Temperature Distribution

Figure 3-3 shows that at detecting point A, which was at the upper part of the bronze cup type D, the temperature was a little lower than 100°C. This may have been caused by the cooling effect of the bronze cup. However, it can be assumed that the bubble was stable and conditions were good for stable arc and weld pools. While at point A', which is at the low part of the cup near to the just solidified metal, the temperature at times rose higher than 100°C meaning overheated gas existed there. At point B', the front bottom of the cup, and point B, at upper part of the front, the temperature was usually much lower than 100°C and the water remained liquid.

Gas cavity shape was related to the heat distribution. The arc column, welding pool, and the just solidified weld were the primary zones where boiling and vaporization of the water occurred. With consideration of the torch movement and the flexible shroud firmly contacting the plate, the gas cavity shape could be predicated. Within the space confined by the shroud, the rear part should have more gas than the front. At the front inner side, heating of the cool water occurred, but the water may have remained liquid if the gas generated was insufficient. At the rear part and over the just solidified hot metal, vapor was still being produced and more gas was collected. If the gas generated was high enough, the gas escaped between the skirt and the work piece.

From this data, a gas distribution model can be drawn as shown in Figure 3-4. Figure 3-5 shows the gas escaping from the ovoid shroud (type E).

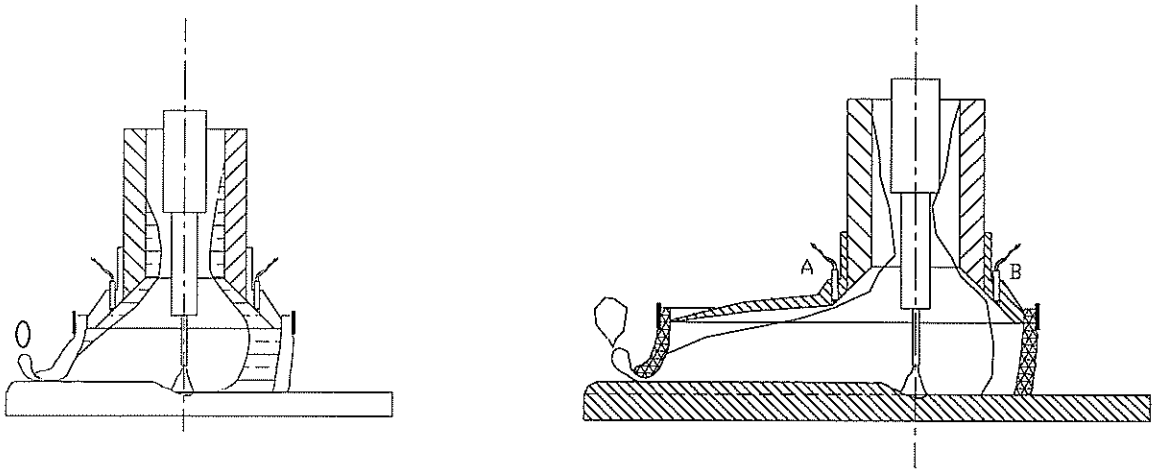

Figure 3-4. Gas Cavity in Shrouds (a) Round Shroud, (b) Ovoid

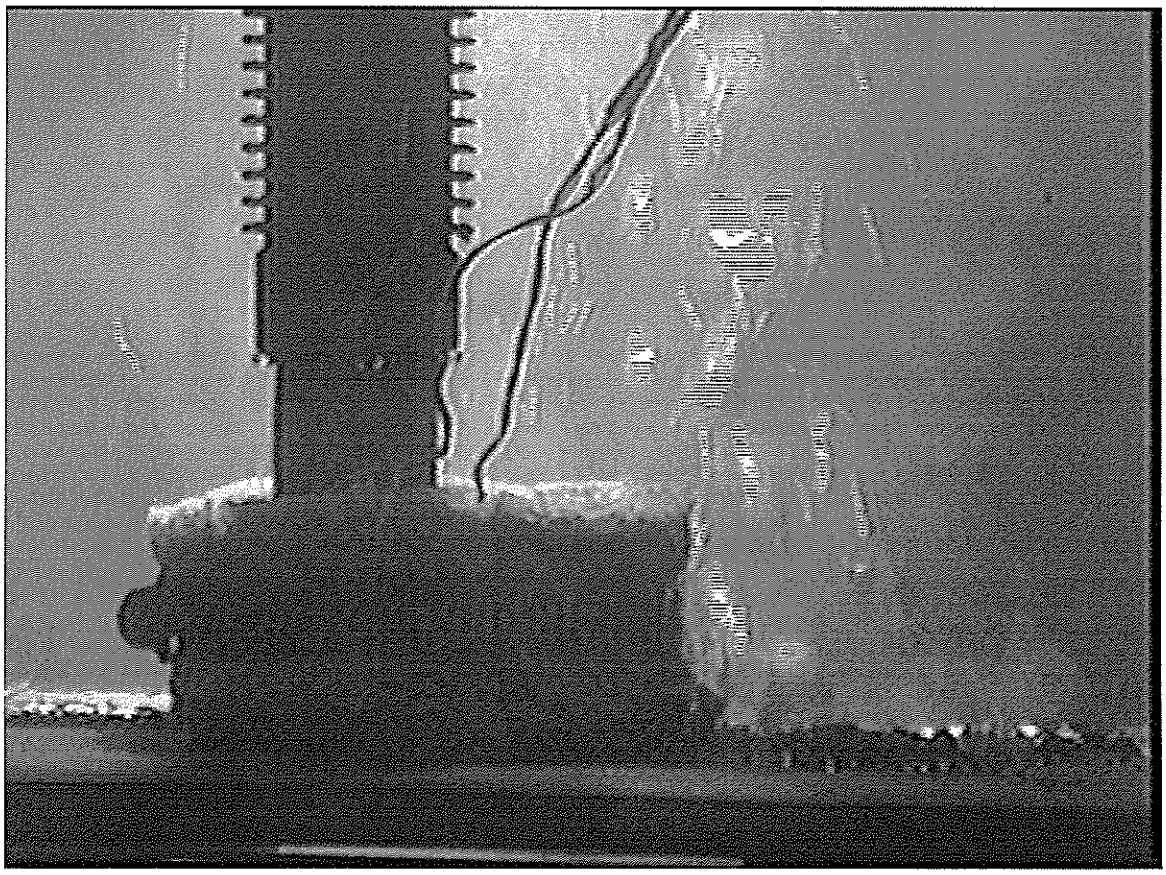

Figure 3-5. Underwater FCAW process with ovoid sponge shroud, no external shielding gas. Two wires beside the torch are leads of thermocouples embeded in the shroud. Gas was lead to the rear part of the shroud to protect pool and weld. Gas escaped from the end of the shroud smoothly in small bubbles.

3.2.3 Effect Of Torch to Workpiece Distance (Shroud Tightness)

Figure 3-6 shows the results of welding tests at different torch to work distances (torch height). It is known that when torch height increases, wire stick out increases and current decreases to maintain melting rate. The decreased arc energy produces less gas and was one of the reasons of lower cavity temperature, but the function of the shroud holding the gas played a more important role. With the designed skirt length, 0.75" was found to be the best torch height, at which the sponge tightly but smoothly contacts the work plate. At the height of 0.625", the skirt was forced to the plate non-uniformly and gas escaped easily and at random position. With too high a torch position, gas also escaped easily from the gap between the skirt and the work piece. Experimental results showed that on flat plate with the chosen shroud design, compression of the sponge 0.1" to 0.2" against the plate had the best results.

file name	Voltage	FeedRate	TorchHight	current	Depth	GasFlow	Ta	Tb	Ta'
(*.dat)	(V)	(ipm)	(in.)	(A)	(in.)		(*C)	(*C)	(*C)
523B		160	0.625	137			85.2		97.6
523C		160	0.750	134			94.8		100.3
523D		160	1.000	120			91.6		95.2

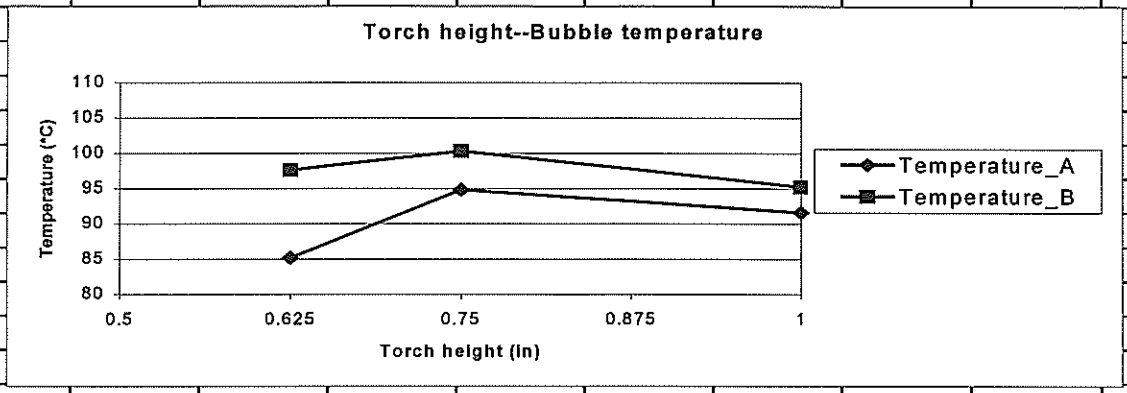

file name	Voltage	FeedRate	TorchHigh	current	Depth	GasFlo	Ta	Tb	Ta'
(*.dat)	(V)	(ipm)	(in.)	(A)	(in.)		(*C)	(*C)	(*C)
523E		200	1.000	154			94.4		97.6
523F		200	0.875	160			96.7		98.9
523G		200	0.750	166			96.5		101.5
523H		200	0.625	174			91.6		101.4

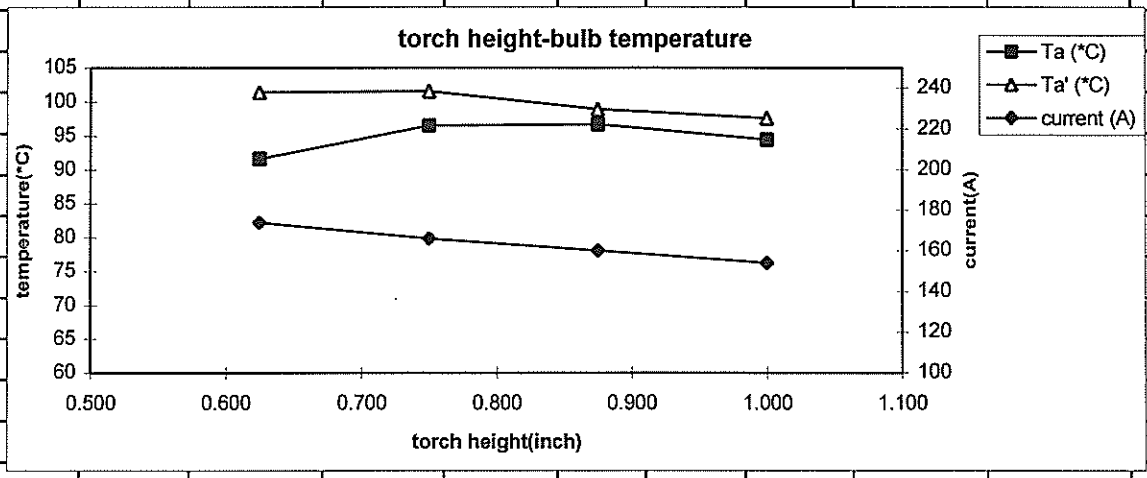

Figure 3-6. Torch Height-Arc Bubble Temperature Relation
Upper: at feed rate of 160ipm;
Lower at feed rate of 200ipm

3.2.4 Effect Of External Gas Flow

Gas cavity temperatures recorded with different external gas flow are shown in Fig.3-7. It was found that the external gas flow had a strong cooling effect. With a flow of 7 cubic feet per hour (cfh), the bubble temperature was highest, but this flow was considered to be low in most cases. With flows of 20 and 40 cfh, the temperature went much lower compared to the temperature with no external gas at the tested current (130A). With higher currents the energy input reimbursed such cooling effects.

file name (*.dat)	Voltage (V)	FeedRate (ipm)	current (A)	TorchHigh (in.)	Deepth (in.)	GasFlo	Ta (*C)	Tb (*C)	Ta' (*C)
616D						0	73.2		75.6
616G						7	89.5		93.5
616E						20	76.1		86.9
616F						40	70.6		81

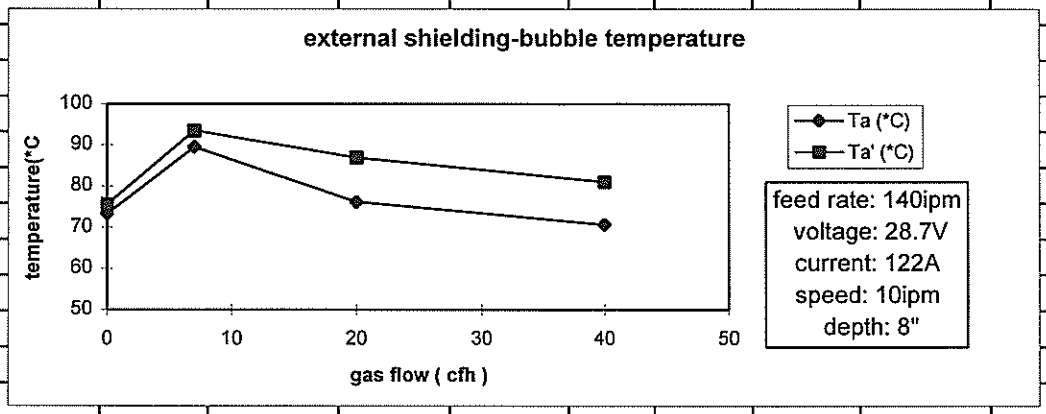

Figure 3-7. External Gas Flow Vs. Gas Cavity Temperature

3.3 Arc Bubble Close Loop Control Results

Figure 3-8 shows the parameter records of bead-on-plate welding tests with closed-loop gas cavity control. It could be seen that after 20~30 seconds the feed rate was optimized to a stable value. With the control system, the gas cavity was maintained stabile. Since the feed rate didn't change wildly, the weld deposited smoothly. Weld appearances are shown in Fig.3-9.

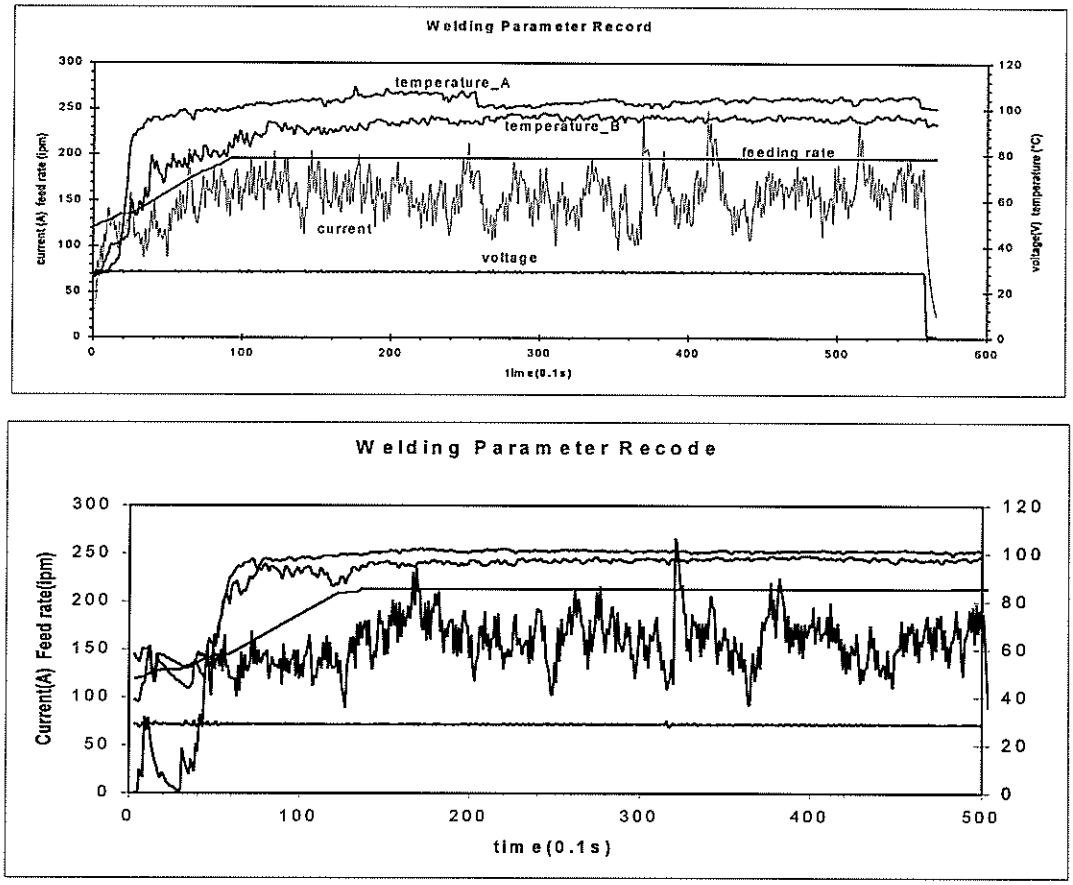

Figure 3-8. Welding Parameters Records With Closed Loop Control

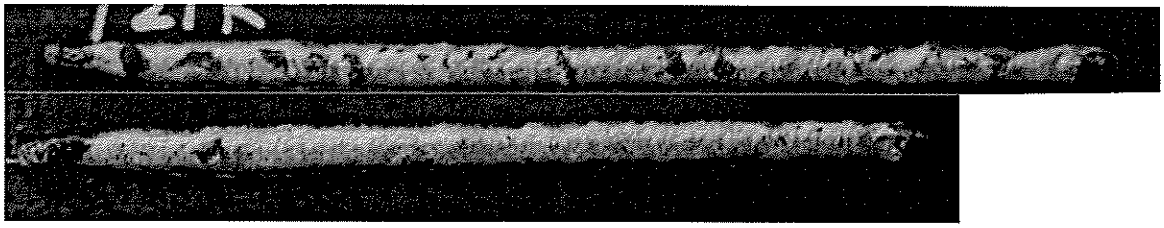

Figure 3-9. Photo of beads-on-plate welded with closed-loop arc bubble control

V-Groove tests results are shown in Figure 3-10 (parameter record) and Figure 3-11 (weld appearance photograph). With V-grooves, gas leaked more than bead-on-plate and higher current was needed to maintain a stable gas cavity. The results showed that the control algorithm and hardware system functioned well.

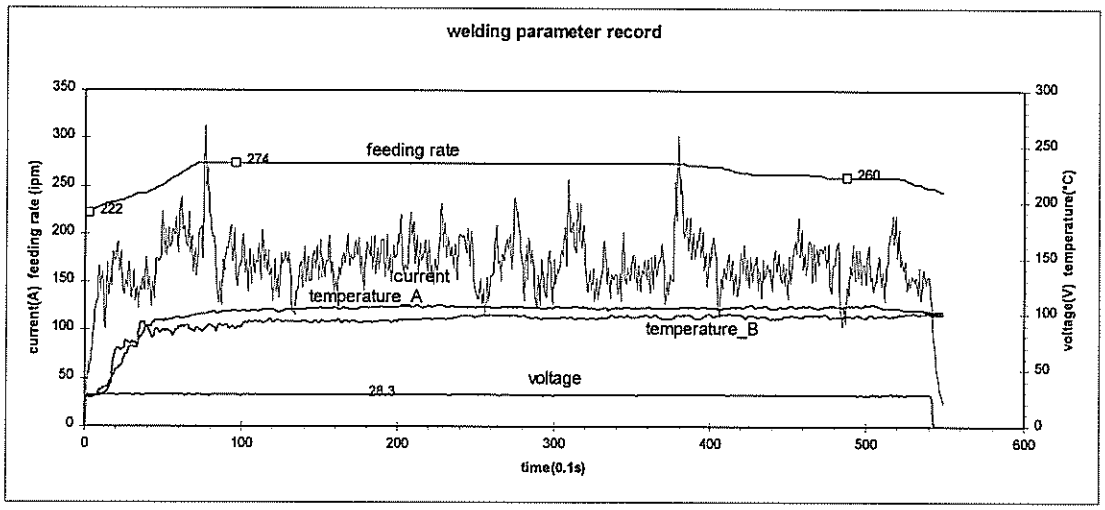

Figure 3-10. Close loop control of gas cavity in welding of V-groove joint

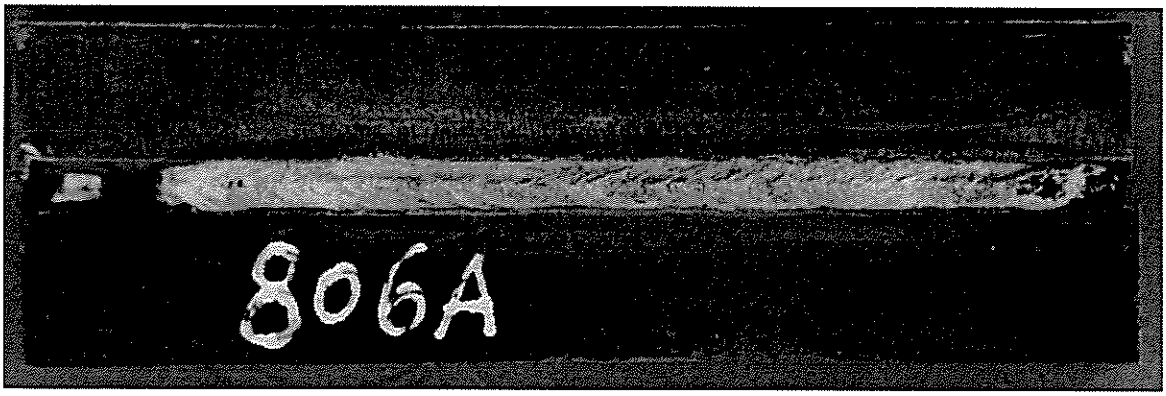

Figure 3-11. Appearance of weld in V-groove joint with gas cavity control

3.4 Effects Of Shroud Design on Cooling Rate and Weld Protection

The shroud design affected both the weld appearance and the cooling rates. The best results were with the ovoid cup as discussed below.

3.4.1 Weld Appearance with Different Cup/Shrouds

Figures 3-12 (a)~(c) show the appearance of welds performed underwater with different arc/weld shielding method at currents of about 175A. When welding with no sponge shroud and 30cfh external air, the gas escaped quickly and the gas cavity surrounding the pool was too small and unstable to shield the weld. The surface of the weld was very coarse and significant porosity existed. With a round sponge shroud (1.75" diameter) and no external gas, the weld profile improved much. Most of the surface was bright and smooth, but some black "scars" still existed, suggesting that water intrusion to the pool existed. With the ovoid sponge shroud, the arc and weld were best shielded and the best weld profiles were obtained. With high current, usually over 190A or feed rate higher than 250ipm, welds of smooth, bright and flat profiles (Figure 3-12(d)) were obtained with this process.

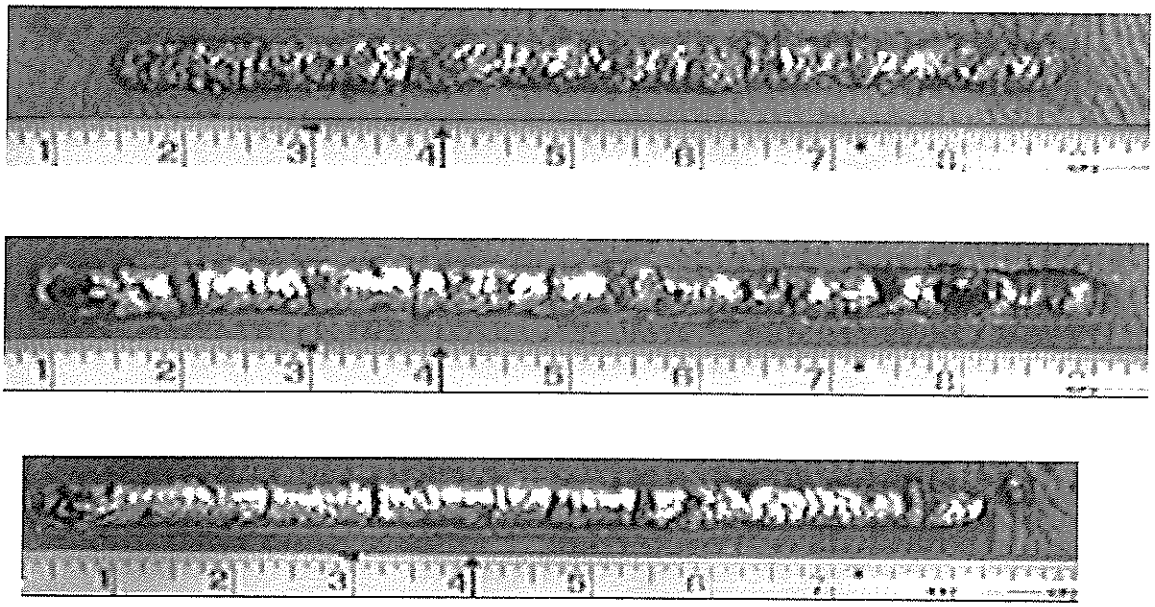

Figure 3-12. Appearance of welds with no shroud, 30cfh air (upper), round shroud (middle), and ovoid shroud (lower)

3.4.2 Cooling Rate Data and Analysis

With above water welding, $T_{8/5}$ was estimated as 4.5 (in second) times as heat input (in MJ/m) according to literature. In under water welding, it was 1.5 to 2.5 times the heat input without special shielding.

The records of thermal variations in underwater welding are shown in Figure 3-13. Table 3-3 lists the test results and calculates average and equivalent value.

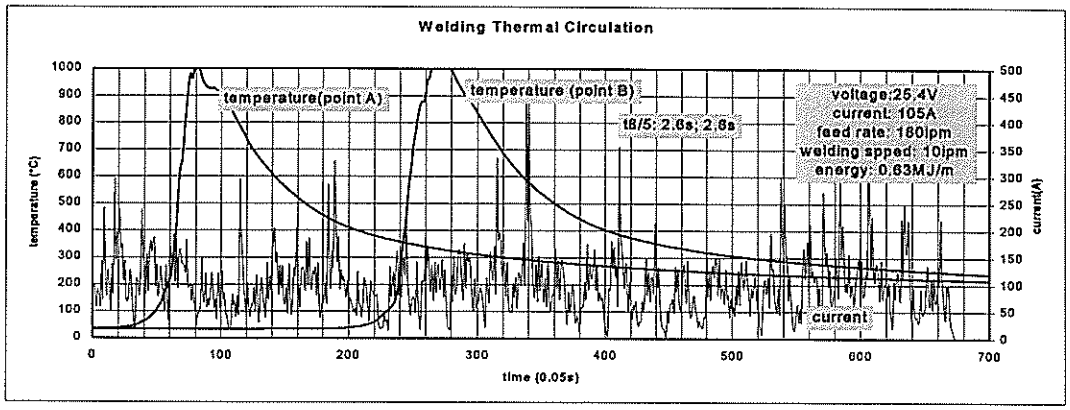

(a)Welding in air with standard nozzle

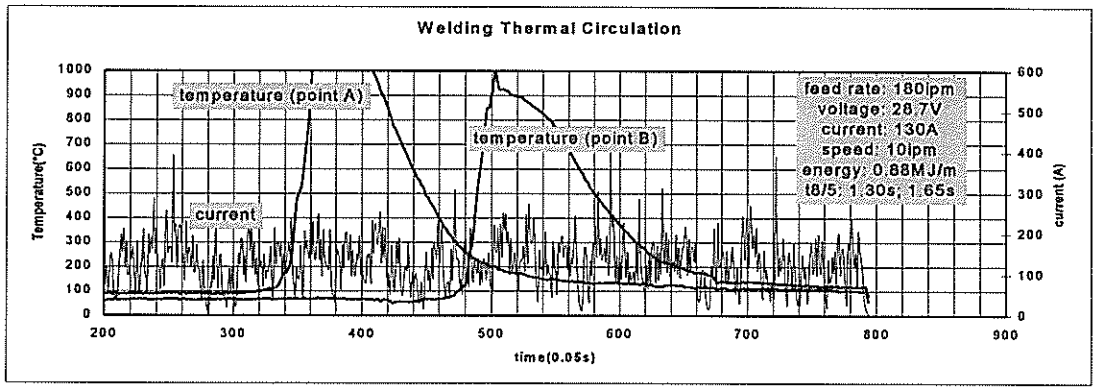

(b) Welding underwater with no shroud (standard in air using nozzle)

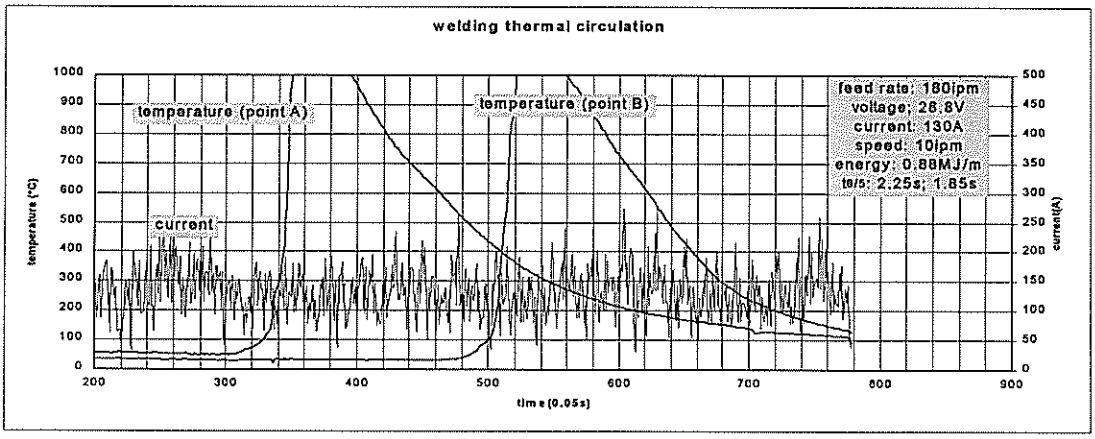

(c) Welding underwater with round shroud

Figure 3-13(a)~(c) HAZ Thermal Circulation with Different Shrouds

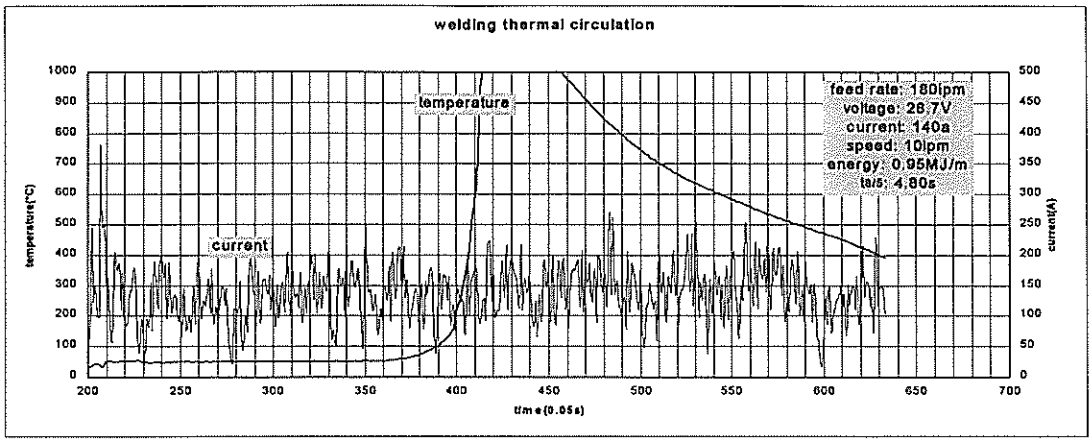

(d) Welding underwater with ovoid shroud

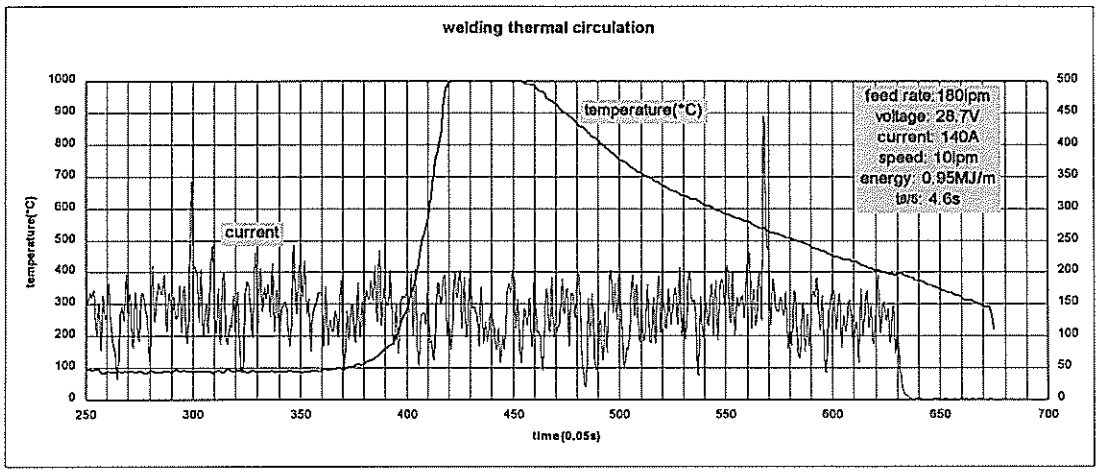

(e) Welding underwater with ovoid shroud

Figure 3-13(d) - (e) HAZ Thermal Circulation with Different Shrouds

Welding Condition	Weld Sample #	Energy Input (MJ/m)	Measured $T_{8/5}$ (second)	Equivalent $T_{8/5}$ (second) (to 1MJ/m)
Miller nozzle in Air, No external gas	717A 811A	0.63 0.95	2.6 0, 2.80 9.2 0, 9.90	**7.1**
Miller nozzle Underwater, 60cfh air	716A	0.88	1.30,1.65	**1.7**
Round shroud, Underwater, No external gas	706B 718D	0.88 0.95	1.85,2.25 3.05,3.65	**3.1**
Egg shape shroud, Underwater, No gas	703A 703B 806C	0.95 0.95 1.50	4.80 4.60 7.30	**4.8**
Egg shape shroud, Underwater, 7cfh air	703C	0.93	4.10	**4.4**
Egg Shape Shroud, Underwater, 70cfh air	223-1 (806A)	1.50	6.10,5.90	**4.0**

Table 3-3 HAZ cooling time with different shroud and external gas flow

In air welding with the standard Miller torch, cooling time $T_{8/5}$ was about 2.7 seconds with 0.63 MJ/m heat input. Another test measured about 9 seconds at higher heat input. Average cooling time equivalent to 1MJ/m heat input is 7 seconds, with a reasonable assumption that $T_{8/5}$ was proportional to heat input.

With underwater welding with the standard Miller nozzle, cooling time $T_{8/5}$ was 1.7 second equivalent to energy input of 1MJ/m. These results were consistent with literature.

With underwater welding with the type C round flexible shroud used in this project, $T_{8/5}$ was about 3.0 seconds. Compared with the standard nozzle the shielding effect was obviously better but still faster than that of air welding.

Underwater welding with the lengthened egg shape shroud resulted in a cooling time $T_{8/5}$ of about 4.8 seconds, very close to air welding.

SECTION 4

WELD QUALITY

4.1 Code Classifications

Weld quality of underwater welds is normally determined in accordance with the ANSI/AWS D 3.6 American National Standard, *Specification for Underwater Welding.* This standard defines four different weld quality classes, these are: Class A, Class B, Class C, and Class O. Class A welds, the highest quality underwater welds, are "intended to be suitable for structural applications". Class B welds are "intended for less critical applications where lower ductility, greater porosity and other larger discontinuities can be tolerated". "Class C underwater welds are intended for applications where the load bearing function is not a primary consideration." "Class O underwater welds are intended to meet the requirements of some other code". Therefore, it makes sense when trying to qualify a new welding procedure and material that the researchers try to qualify the procedure to the class A underwater welding standard.

4.2 Effect of Gas Nozzle Design on Porosity

To reduce the amount of porosity in the weld metal and thereby increase the weld quality, the bubble around the weld needed to be made more stable. The cooling rate of the weld and HAZ needed to be slower and the water had to be excluded from the arc zone. In order to make the bubble around the welding process more stable and to lower the cooling rate of the weld metal and the HAZ a new gas nozzle was developed. Three differently shaped gas nozzles were tried. The first gas nozzle tried was the gas nozzle that came with the torch, referred to in this report as the standard nozzle. The second nozzle used was a round cup that surrounded the arc. The third nozzle used was an ovoid shaped gas cup. The round gas cup and the ovoid cup were designed to be installed on the torch in place of the standard nozzle.

Thermocouple measurements showed that the cooling rate of the HAZ was the slowest for the ovoid shaped gas cup, so further development was done with this cup. The first set of samples that were made using the ovoid cup and no added external air showed some porosities in the X-rays, as shown in Figure 4-1.

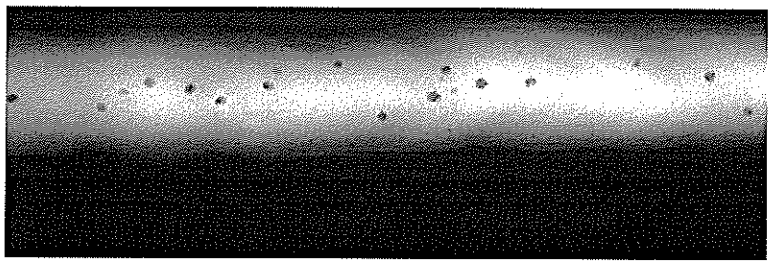

Figure 4-1. X-ray of sample
Ovoid cup no external air

4.3 Addition of Externally Supplied Air

Supplemental air was added to the gas cup in an attempt to exclude the water from the cup and to reduce the number of porosities. Unexpectedly, adding 30 cfh of air to the cup resulted in more porosity than in the samples with no external air as shown in Figure 4-2.

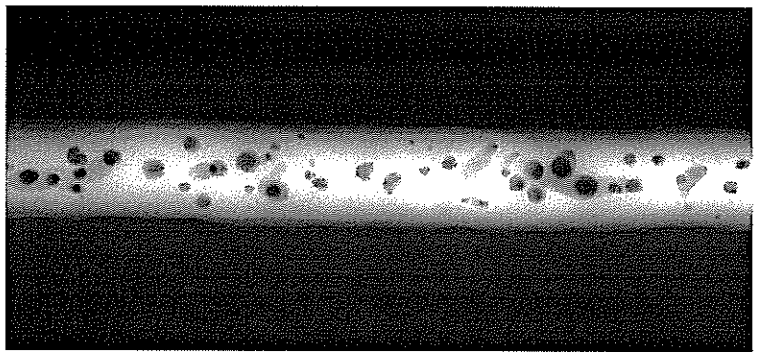

Figure 4-2. X-ray of sample
Ovoid cup + 30 cfh air

There are several possible reasons to explain why adding 30 cfh of air produced more porosity than no external air. One possibility is that the external air stirred the weld pool producing more degassing of the weld metal. However, the addition of 30 cfh of air may not have stirred the pool fast enough to allow the extra gasses to escape before weld pool solidification.

Another possible reason is that the 30 cfh of external air was not enough to exclude the water completely from the gas cup. However, it may have been enough to increase the cooling rate due to convective cooling of the weld surface, trapping the gasses in the bead. A similar phenomena was discussed by Tsai et al[1] in 1979 in *Mechanisms of Rapid Cooling in Underwater Welding* regarding an increase in cooling rate as the minimum bubble radius (R_o) was increased until a minimum value. Increasing R_o past that point decreased the cooling rate.

The addition of 70 cfh of air to the ovoid gas cup virtually eliminated the weld metal porosity while slowing the cooling rate in the HAZ enough to improve HAZ properties (see Figure 4-3).

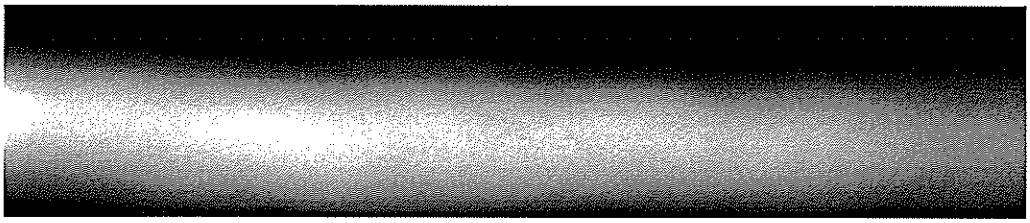

Figure 4-3. X-ray of sample
Ovoid cup + 70 cfh air

4.4 Cooling Rate Effects

4.4.1 $T_{8/5}$ Comparison

A set of welds was also made in air to compare with the underwater welds. The cooling rates of all of the welds were measured in the heat affected zones by installing thermocouples where the HAZ of the welds would be. The time it took for the temperature of the HAZ to fall from 800 °C to 500 °C ($T_{8/5}$) was measured. With an energy input of 1 MJ/M, the $T_{8/5}$ of the in air weld was 4.3 to 9 seconds(see Table 3.3). For the underwater wet weld with standard nozzle the $T_{8/5}$ was 1.7 seconds. The $T_{8/5}$ of the wet weld with the round nozzle welds was 3.1 seconds, and with the oval nozzle it was 4.8 seconds.

4.4.2 Hardness Trace

The increase in the time required for the temperature to fall from 800 °C to 500 °C from the standard nozzle to the ovoid cup reduced the hardness in the HAZ to values similar to the values for in-air welds (see Figure 4-4). This represents a significant improvement in weld quality.

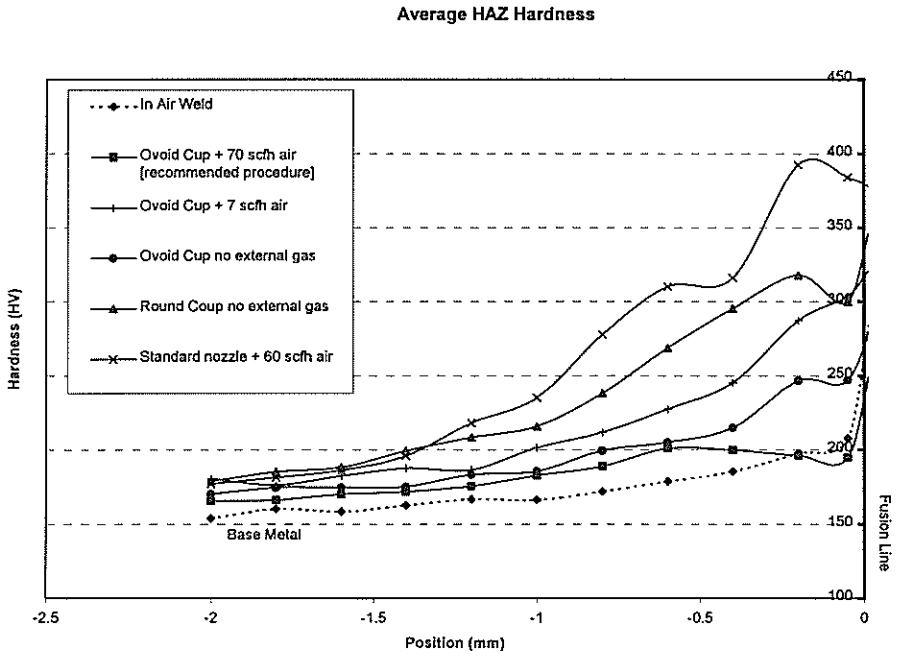

Figure 4-4. HAZ Hardness Traces

4.4.3 Microstructures

The samples were polished using standard metallographic techniques. Samples were then etched using either 2% nital or Kourbatoff no. 4 reagent (10 parts 4% nital and 1 part 4% picral) for the carbon steel base metal. Etching of the carbon steel was then followed by an electrolytic chromic acid etch for the stainless steel weld metal. This process reveals both microstructures at the same time. The samples were repolished after completion of the evaluation to ensure that the artifacts shown were not introduced in the metallographic process. The samples were optically observed and photographed both before etching and after etching with 10% oxalic acid electrolyticly the stainless steel weld metal.

The microstructures of the HAZ in the weldments corroborated the hardness trace data showing a decrease in the amount of martensite as cooling time increased as Figures 4-5 through 4-7 show.

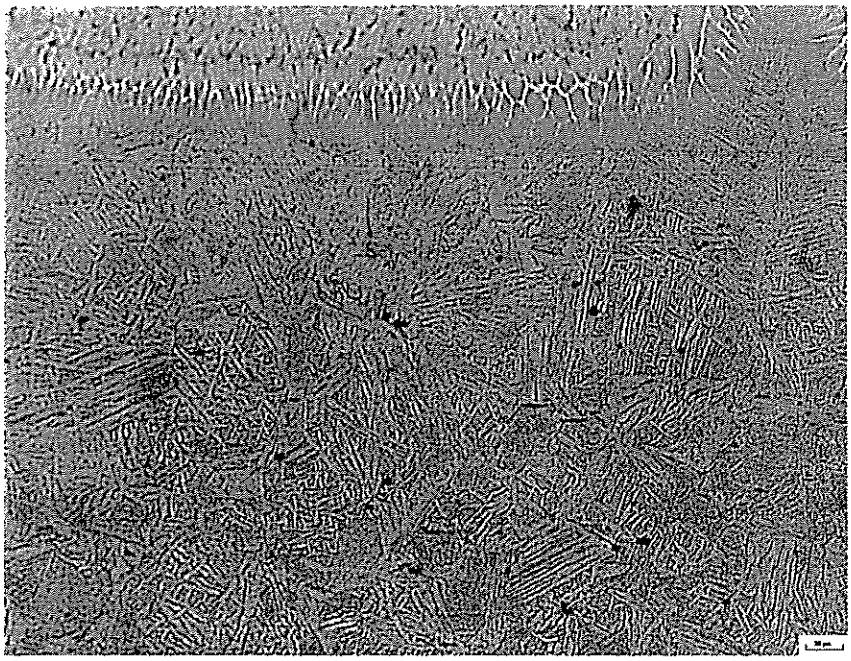

Figure 4-5 HAZ Microstructure, Ovoid cup no external gas
$T_{8/5}$ = 4.8 sec, Energy Input 0.95MJ/M

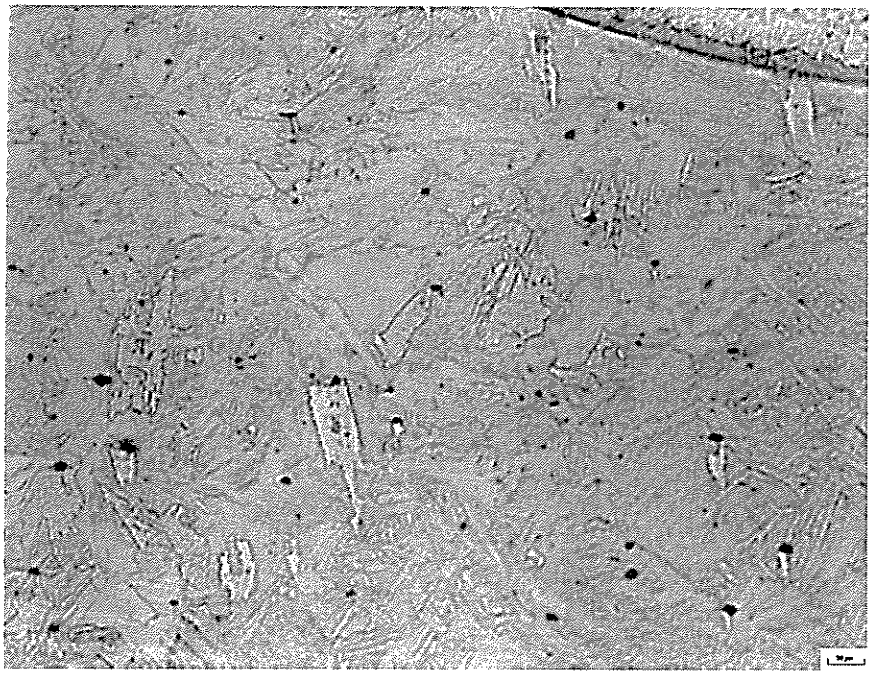

Figure 4-6 HAZ Microstructure, Ovoid cup + 70 cfh air
$T_{8/5}$ = 6 sec, Energy Input .1.5MJ/M

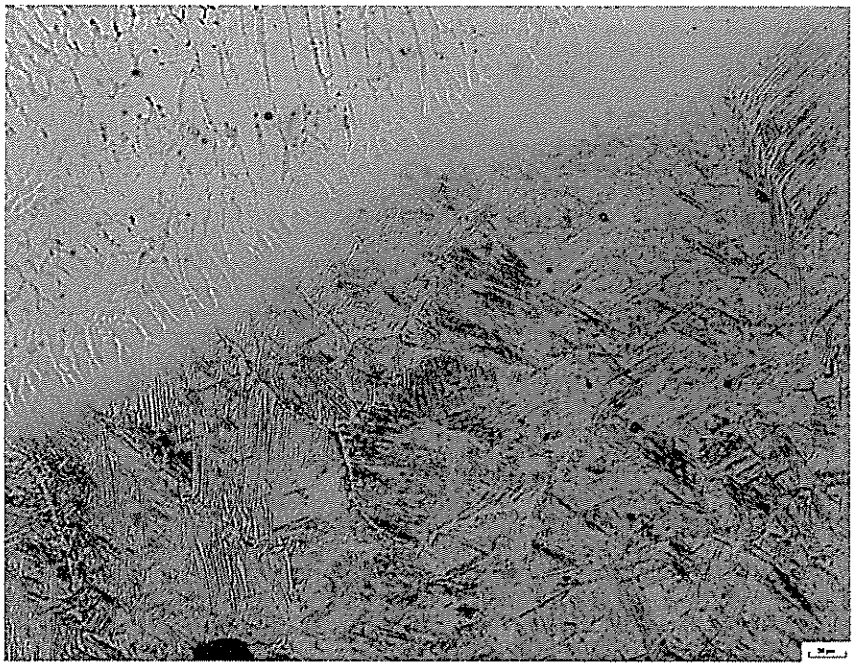

Figure 4-7 HAZ Microstructure, Standard nozzle + 60 cfh air
$T_{8/5}$ = 1.47 sec, Energy Input 0.88MJ/M

4.5 Weld Metal Composition

4.5.1 Bulk Weld Metal

The weld metal composition for the fusion zone of the welds was determined by the composition of the weld metal, the composition of the base metal, and the weld metal dilution. The dilution was a measure of the amount of base metal that was melted in relation to the amount of weld metal melted and is reported in per cent. The underwater wet welds were low dilution welds ranging between 20 and 35 per cent, depending on the heat input. The predicted weld metal microstructure for stainless steels can be determined using the Scheffler diagram. The chrome equivalent and nickel equivalent are determined from the composition of the filler and base metals. These compositions are plotted on the diagram. A tie line was drawn between the two compositions. The dilution is used to determine where along the tie line the resultant bulk

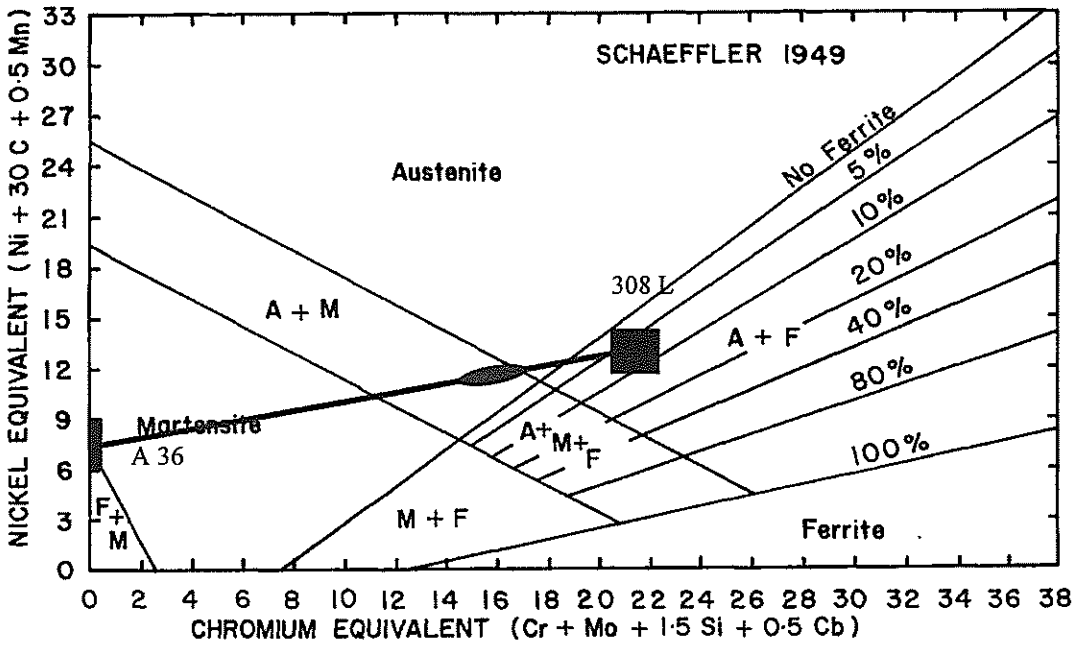

Figure 4-8 Scheffler Diagram

weld metal composition was. The predicted microstructure of the weld metal was read from the graph as shown in Figure 4-8. The actual microstructure of the composite weld metal is shown in Figure 4-9 and agreed with the predicted bulk weld microstructure.

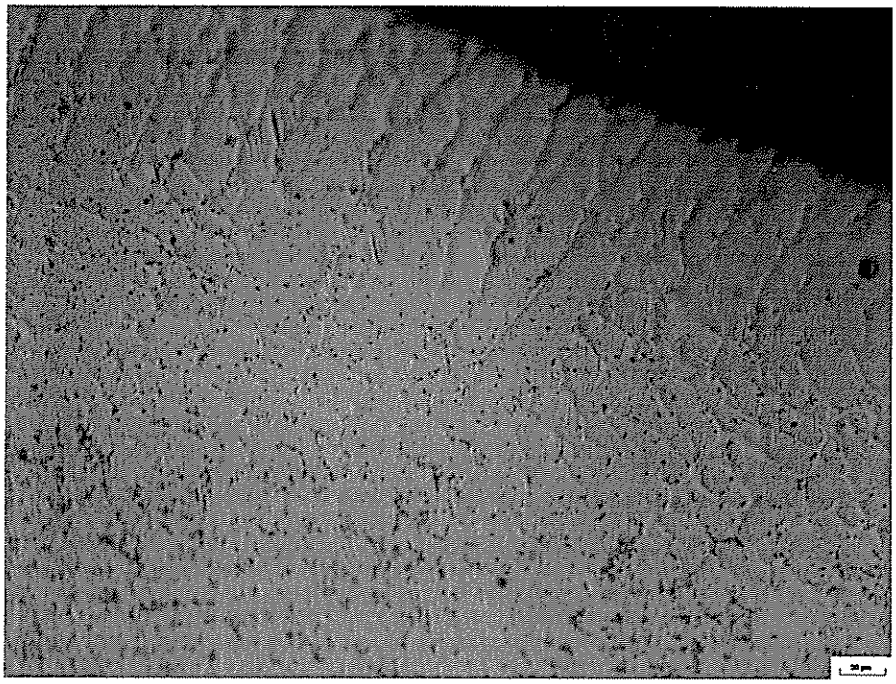

Figure 4-9 All Weld Metal -- Top Surface

4.5.2 Transition Zone

Note that while the bulk weld metal composition can be estimated by the amount of dilution, the transition region cannot. The transition between the A 36 and the 308 L in the weld metal shows layers where there has been incomplete mixing of the weld metal and the base metal in the molten state as shown in Figures 4-10 and 4-11.

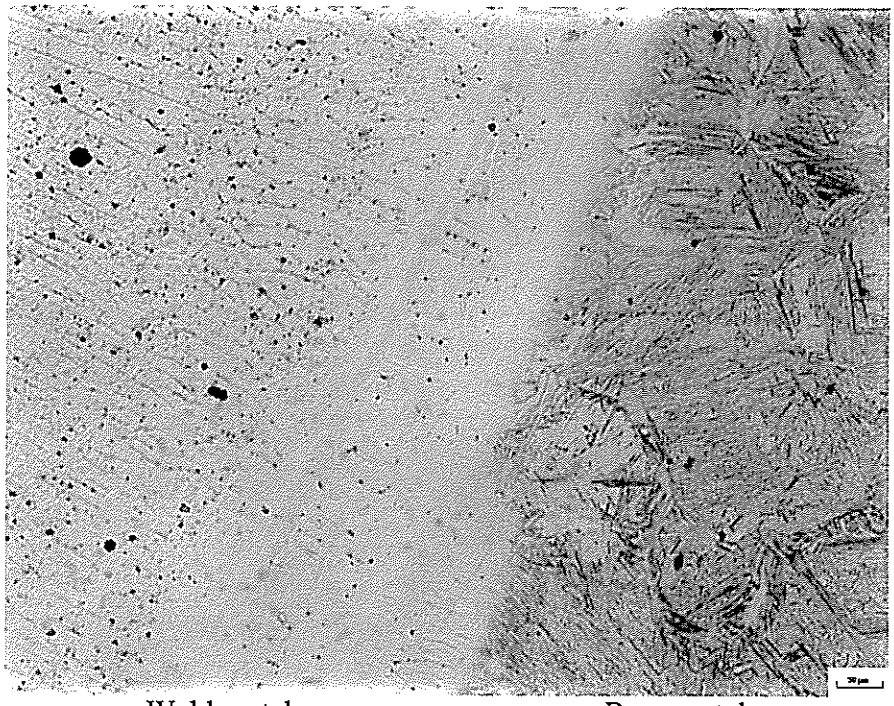

Figure 4-10 Transition zone

Figure 4-11 Transition Zone
Ovoid cup + 70 cfh air

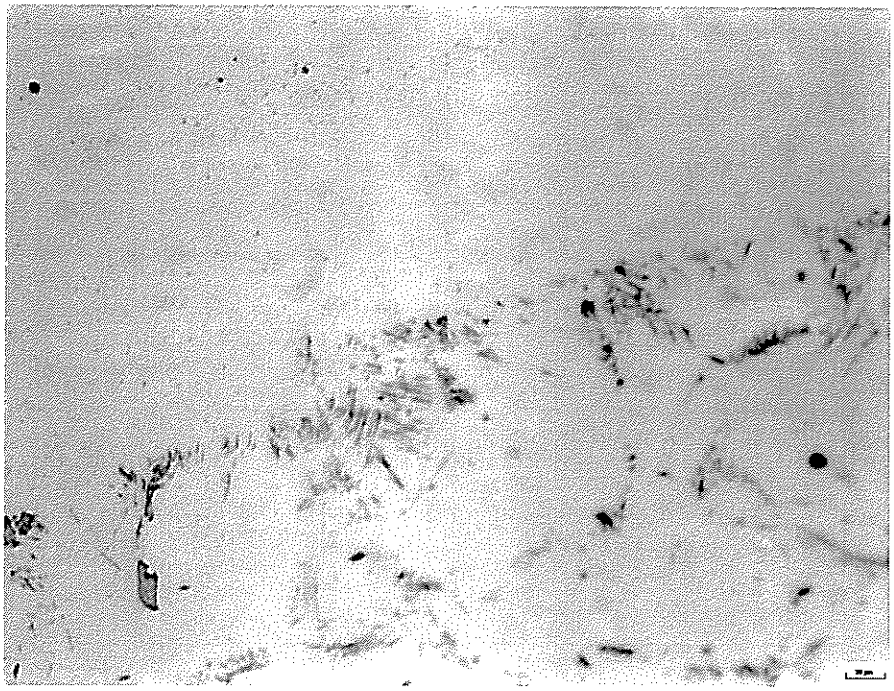

Figure 4-12 Transition zone -- no etch

Even with no etch the transition zone showed as a distinct area, devoid of the inclusions and micro-porosities visible in the HAZ and in the composite weld metal as shown in Figure 4-12.

4.5.3 Mixing

An explanation of manufacturing techniques for 308L flux core wire may help to explain the unusual variations in composition. The industry standard for the construction of Type 308L FCAW wire is to use a sheath of Type 304L stainless steel surrounding the flux and alloys required to make the deposited weld metal have 308L chemistry. This means that complete mixing of the weld metal while it is in the molten state is required to result in the proper chemistry in the weld zone. Those samples of underwater welds having faster cooling rates showed incomplete mixing in the weld zone. This resulted in the variations in hardness in the weld zone. The use of the ovoid shaped cup and 70 cfh of external air allowed the molten weld zone to mix more completely. This resulted in a more homogeneous weld metal composition, smoothing out the hardness variations as shown in Figure 4-13.

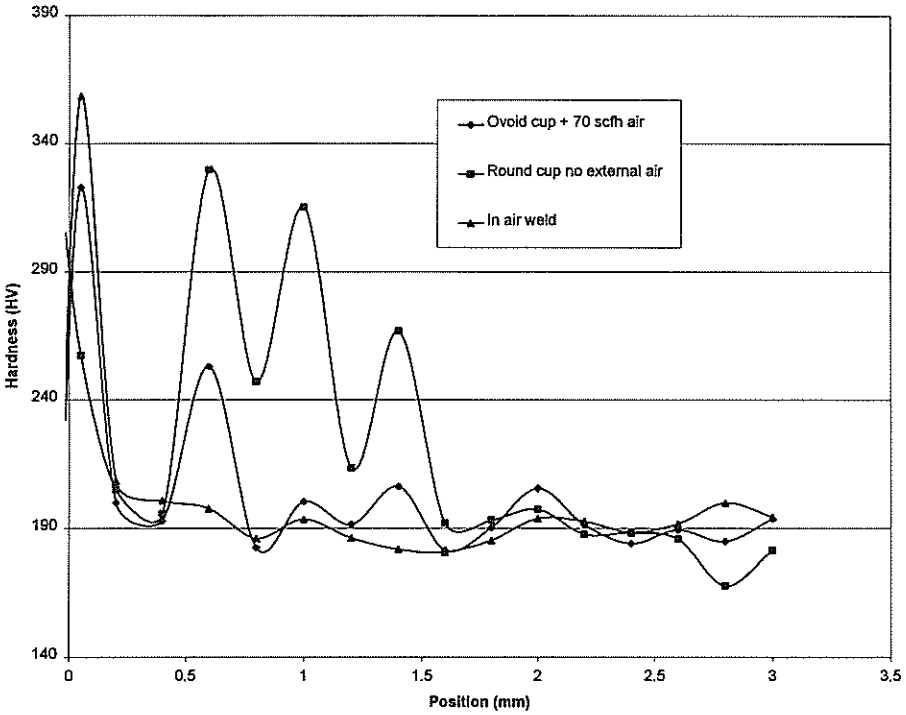

Figure 4-13 Weld Metal hardness
(Individual traverses)

4.6 Mechanical Tests

The welds were done in approximately 6" of fresh water in the small test tank at The Ohio State University Welding Engineering Laboratory. The welds were Flux Cored Arc Welded 308L Stainless Steel with A-36 base metal.

4.6.1 Bend Tests

Bend tests for the development of the control algorithm showed that the ductility of the materials was extremely dependent on the amount of porosity and/or the number of inclusions in the welds as shown in Figures 4-14 and 4-15.

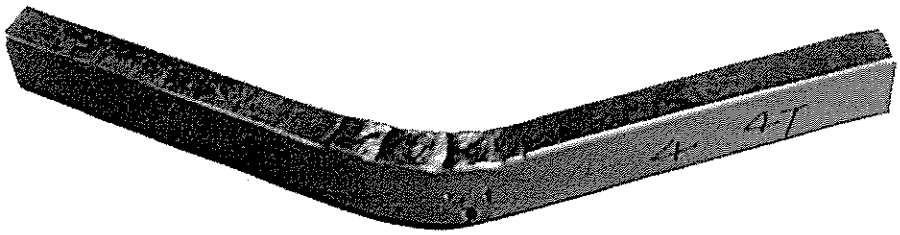

Figure 4-14 Side bend with porosities in the weld metal
2T radius bend 40° angle

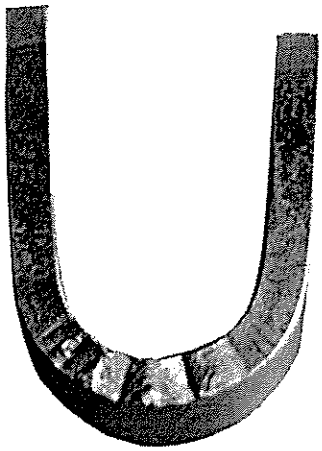

Figure 4-15 Side bend without porosities in the weld metal
2T radius bend 180° bend

4.6.2 All Weld Metal Tests

All weld metal tensile tests on the 308L weld metal used for control algorithm development showed a yield strength of 69.7 ksi and a UTS of 87.1 ksi with an elongation of 25.5%. The required elongation of an all weld metal tensile test for a Class A underwater weld was 19% for the A-36 base metal used in this project (yield strength less than 50 ksi). Figure 4-16 shows the graph of the tensile test results.

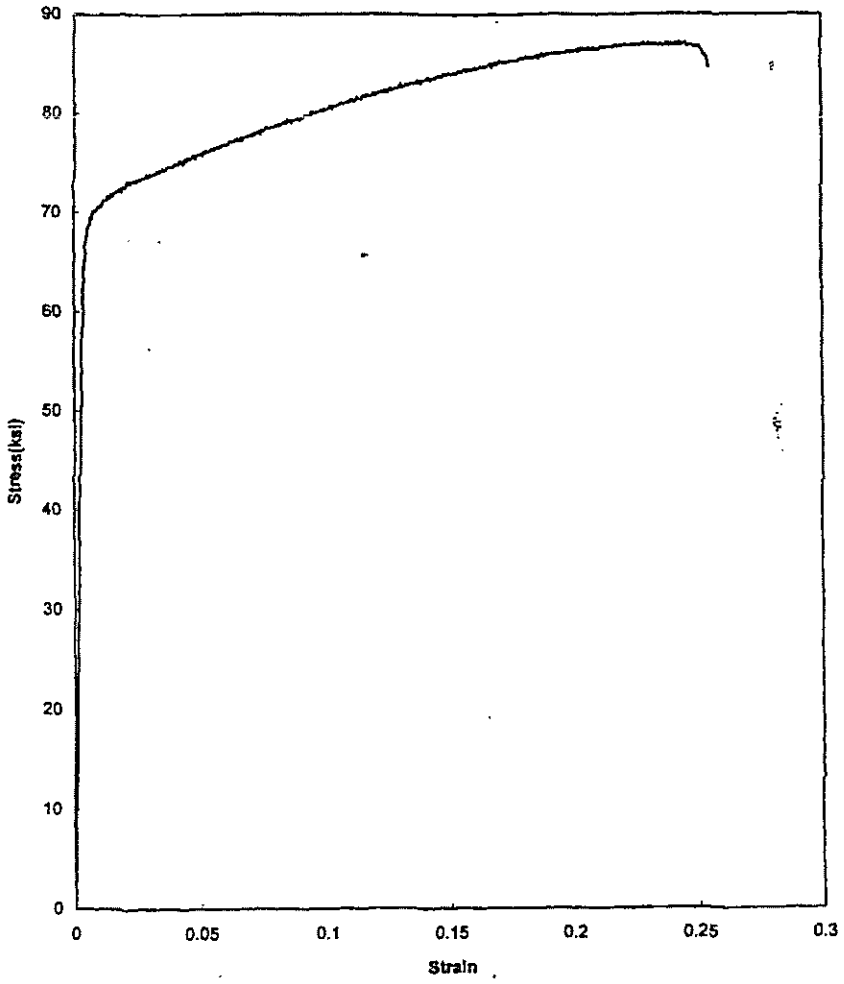

Figure 4-16 AWM Tensile test results
308 L weld metal

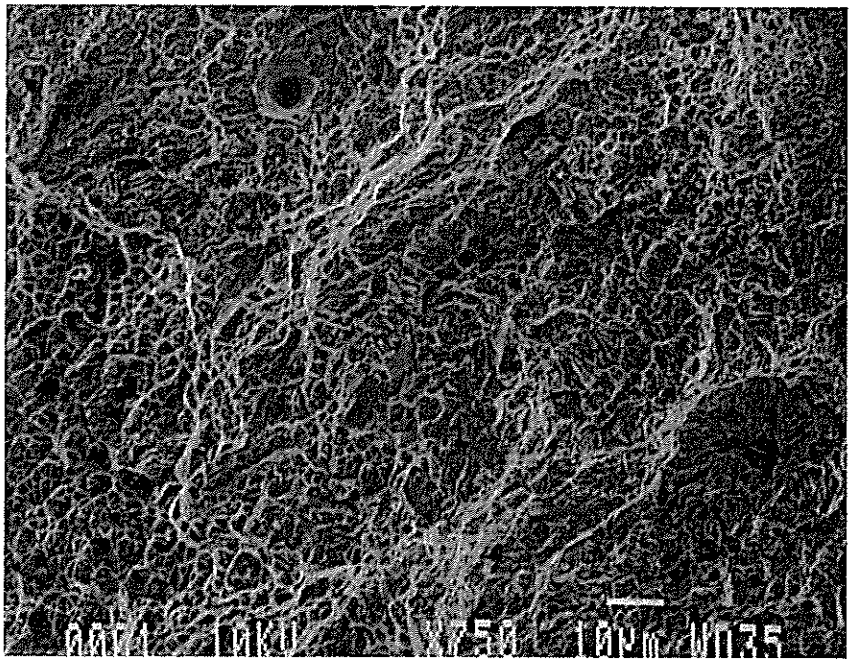

Figure 4-17 Ductile and quasi-clesavage failure
AWM tensile test fracture surface

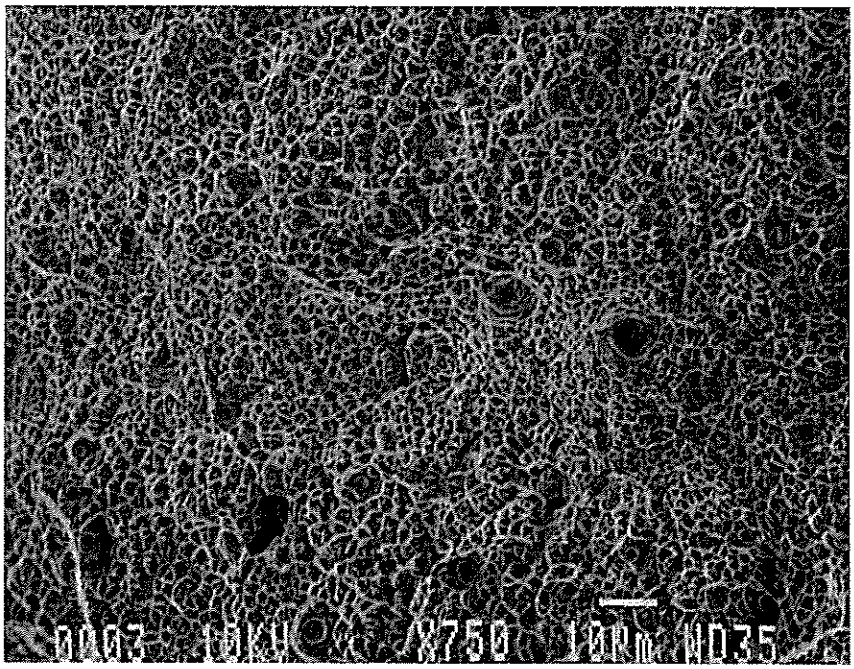

Figure 4-18 Ductile failure
AWM tensile test fracture surface

4.6.3 Fracture Analysis

The fracture surfaces of the tensile test bars showed the cone and cup fracture morphology that is indicative of a ductile fracture in some areas. In other areas they showed a combination of ductile and quasi-cleavage morphology as shown in Figures 4-17 and 4-18. The mixed mode fracture is believed to be due to dissolved hydrogen in the weld metal since the cooling rates and hardnesses approximate those of air welds.

SECTION 5

CONCLUSIONS

Conclusions

1). An analysis of microstructures and mechanical properties showed that satisfactory underwater welds could be made using Stoody 308L SOS flux-core wire on A36 mild steel using the local dry spot method. The improved weld quality was obtained by developing a microprocessor based data acquisition/processing system to monitor/control the gas cavity (bubble) stability and status in real time to better protect the arc and weld. Thermal data from sensors in the shroud were converted to a gas bubble status message. A semi-empirical relationship between the bubble status message, welding parameters, and weld quality was established. The control algorithm hardware was developed by using feedback principles and the database. The wire feed rate was controlled in real time to adjust energy input and hence the amount of gas from the flux and vaporization.

2). Because of the significant effect of cooling rate on weld properties/microstructures, shroud design was evaluated and a new shroud was developed to slow the cooling rate. It was ovoid in shape, as are the isotherms surrounding the weld pool. The ovoid shape allows the gas shield to flow backwards along the weld centerline to more efficiently shield the weld pool and solidified metal. With the ovoid cup and closed loop system, good bead profiles and sound microstructures were consistently produced. The cooling rate ($T_{8/5}$) was slowed to 4 - 6 seconds from 1.7 seconds, resulting in highly improved hardness' and microstructures.

3). No cracking was observed in either the weld metal or the heat affected zones when using the ovoid cup.

4). The peak hardnesses were on the weld zone side of the fusion line in the transition region from 308L weld metal to the A36 base metal. Variations in hardness across the weld bead indicate some incomplete mixing of the 304 sheath of the 308L wire and the alloying elements in the flux. With the developed process and parameters, the mixed zone situation was improved, peak hardness' and hardness variations in the transition zone were lowered to satisfactory levels.

5). Bend test coupons were able to pass a 2t radius (4t diameter) bend when no slag inclusions or significant porosity existed.

6). A new ovoid cup with a 30 degree drag angle has been developed to reduce the chance of slag inclusions and to operate the process with the proper drag angle. Testing of the cup has not yet been performed, but it is expected to perform even better.

SECTION 6

SUGGESTED CONTINUING WORK

6.1 Welding in the Dive Tank

Weld qualification testing still needs to be accomplished in the diving tank. Due to the loss of an available diver and the moving and refurbishing of the dive tank, this task has been delayed. In the event that a suitable diver cannot be secured to perform the work, a mechanized system will be constructed to perform the welding. Class A quality welds in the flat position will be attempted, and it is anticipated that all requirements will be met.

6.2 Mechanized Welding in the OSU Diving Tank

Mechanized welding in the dive tank with the integration of a tracking/Inspecting System is also recommended. A remote camera installed in the cup can be used to help track the joint. This can later be integrated with a virtual vision system combining through arc sensing information with visual tracking.

6.3 Underwater FCAW Torch and Wire Feeder Development

A commercial underwater FCAW Torch needs to be developed to extend the range to below 10 feet. Modification and waterproofing of a small spool gun mechanism and integration with the feedback loop control and virtual vision system would provide the required flexibility in open water and would provide weld quality meeting Class A code requirements for many applications. Mechanization of the process using tracking systems like those used on orbital GMAW welding of pipe and carriage systems for linear welds such as for submerged arc would better insure weld quality for critical applications.

REFERENCES

1. Tsai, Chon L. and Koichi Masubuchi. *Mechanisms of rapid cooling in underwater welding.* Applied Ocean Research, Vol. 1, No.2, 1979.

2. Tsai, Chon L. and Koichi Masubuchi. *Mechanisms of rapid cooling and their design Considerations in Underwater Welding.* Journal of Petroleum Technology, October, 1980.

3. Atkins, M. *Atlas of continuing cooling transformation diagrams for engineering steels.* American Society for Metals, revised U.S. edition, 1980.

4. ASM. *Atlas of isothermal transformation and cooling transformation diagrams.* American Society for Metals. March, 1977.

5. Tsai, Chon L. et al. *Development of and Underwater SMAW Electrode for Improved Fatigue Strength in Wet Welded Joints.* Ohio's Thomas A. Edison Program, Edison Seed Development Fund Technical Report, The Ohio State University, Columbus Ohio, June 1991.

6. Tsai, Chon L, and Jiang, Chong H. *Verification and Dissemination of the Required Engineering Data Base for the New Underwater, Flux-Coated Welding Electrode in Commercial Applications.* An NCRI Final Report, OSU RF Project # 727962. Ohio State University, Columbus, OH 43210, Dec 95.

7. Tsai, Chon L., et. al. *Engineering Assessment of Weld Joint Design for Underwater "Wet" Welding.* Navy Joining Center final report. The Ohio State University, Columbus, Ohio March 1995.

8. American Welding Society. *Specification for Underwater Welding.* AWS D3.6 - 93, American Welding Society, Inc., Miami, FL 33135, 1993.

9. Tsai, Chon L., Chong H. Jiang, and Daein Kang. *Development of a Smart Underwater "Wet" Welding Process Ohio Sea Grant College Program* . The Ohio State University, RF #729734 Final Report, October 31, 1996.